

Bifunctional Small Molecules That Mediate the Degradation of Extracellular Proteins

David Caianiello, Mengwen Zhang, Jason Ray, Jake Swartzel, Emily Branham, Egor Chirkin, Venkata Sabbasani, Angela Gong, David McDonald, Viswanathan Muthusamy, David Spiegel

Submitted date: 03/08/2020 • Posted date: 04/08/2020

Licence: CC BY-NC-ND 4.0

Citation information: Caianiello, David; Zhang, Mengwen; Ray, Jason; Swartzel, Jake; Branham, Emily; Chirkin, Egor; et al. (2020): Bifunctional Small Molecules That Mediate the Degradation of Extracellular Proteins. ChemRxiv. Preprint. <https://doi.org/10.26434/chemrxiv.12732689.v2>

Targeted protein degradation (TPD) has emerged as a promising and exciting therapeutic strategy. The majority of existing TPD technologies rely on the ubiquitin-proteasome system, and are therefore limited to targeting intracellular proteins. To address this limitation, we developed a class of modularly designed, bifunctional synthetic molecules called MoDE-As (Molecular Degraders of Extracellular proteins through the Asialoglycoprotein receptor (ASGPR)), which are capable of mediating the degradation of extracellular proteins. MoDE-A molecules mediate the formation of a ternary complex between a target protein and the ASGPR, which is expressed primarily on hepatocytes. The target protein is then endocytosed and degraded by lysosomal proteases. We demonstrated the modularity of the MoDE-A technology by synthesizing bifunctional molecules that induce the degradation of both antibody and pro-inflammatory cytokine proteins. To our knowledge, these data represent the first experimental evidence that non-proteinogenic, synthetic molecules can be employed for the TPD of extracellular proteins both in vitro and in vivo. We believe that TPD mediated by the MoDE-A technology will have widespread applications for disease treatment.

File list (2)

20200728 Supp .pdf (1.45 MiB)

[view on ChemRxiv](#) • [download file](#)

20200731 main.pdf (1.28 MiB)

[view on ChemRxiv](#) • [download file](#)

Supplementary Materials for

Bifunctional small molecules that mediate the degradation of extracellular proteins

David F. Caianiello, Mengwen Zhang, Jason D. Ray, Jake C. Swartzel, Emily M. J. Branham,
Egor Chirkin, Venkata R. Sabbasani, Angela Z. Gong, David M. McDonald, Viswanathan
Muthusamy, David A. Spiegel*

*Correspondence to: david.spiegel@yale.edu

This PDF file includes:

Biological Materials and Methods
Synthetic Methods
Figs. S1 to S4
Spectral Data
Full reference list

Biological Materials and Methods

Data was analyzed and visualized using GraphPad Prism 7.0a software.

Cell culture

HepG2 cells were purchased from ATCC. Cells were cultured in RPMI medium 1640 (Gibco, Ref 11875) supplemented with 10% FBS (Millipore Sigma, TMS-013-B) and penicillin/streptomycin (ThermoFisher, 10378016). Assays were carried out in sterile-filtered opti-MEM (Gibco 31985-070) supplemented with 0.1% BSA (Sigma, A9418) and penicillin/streptomycin. Cells were grown to greater than 90% confluency before beginning all experiments. Cells were passaged by first aspirating the media, followed by treatment with trypsin (0.25%, Gibco ref 25200) and incubation at 37 °C until cells began to detach from the plate (approximately 5 minutes). Cell aggregates were dispersed by passing the cell solution through a 200 μ L pipette tip several times.

Biological Reagents

Asialofetuin (Sigma, A4781), fetuin (Sigma, F2379), and ORM (Sigma, G9885) were each resuspended at a concentration of 1 mg/mL. ASOR was prepared from ORM using a solid-phase neuraminidase kit (Sigma, N5254). 15 mg of ORM was treated with immobilized neuraminidase corresponding to 0.5 units. The kit defines 1 unit as the amount of enzyme necessary to remove 1.0 μ mol of sialic acid from bovine submaxillary mucin in 1 minute at pH 5 and 37 °C. Desialylation was carried out in a buffer of 100 mM sodium acetate and 2 mM calcium chloride (pH 5) according to manufacturer instructions. Briefly, the slurry of neuraminidase beads was placed on filter paper, then dried over vacuum. The filtrate was washed with DI water 10 times before the beads were added to the ORM solution. The neuraminidase beads were then incubated with ORM on a rotator for 1 hour at 37 °C, followed by filtration to remove the neuraminidase and dialysis against PBS overnight at 4 °C. Removal of sialic acid was confirmed using a sialic acid assay kit (Sigma, MAK314). *In vitro* experimentation with D-MoDE-A was performed with an α -DNP-KLH rabbit IgG fraction conjugated to Alexa Fluor 488 (AF488) (Thermo, A11097). MIF (Cayman, 14493) was fluorescently labeled using an AF488 antibody labeling kit (Thermo, A20181). A single tube of dye was used to label 24 nmol (300 μ g) of MIF protein. Unreacted dye was removed by using size exclusion zebra spin columns with a 7k MWCO filter (Thermo, 89878).

Ternary complex formation assays

Flow experiments were performed using an Accuri C6 flow cytometer using BD Accuri C6 software. Data was analyzed using FlowJo version 10.4.2 for Mac. All incubations for ternary complex assays were carried out on ice to halt the endocytosis of cell-surface proteins (46). Cells were removed from culture plates by treatment with 1 mM EDTA/1 mM EGTA solution in PBS (prepared in house) for 20 minutes at 37 °C. The cells were then pelleted (7 minutes, 300 \times g), and resuspended in ice-cold assay media to replenish calcium. Cells were pelleted and resuspended in media three further times. Aliquots of approximately 35,000 cells were used for each individual experiment. Cells were aliquoted into a 96-well U bottom plate and treated first with α -DNP (to a final concentration of 100 nM), then compound. The cells were mixed gently via pipette, and incubated on ice for 30 minutes. Cells were then mixed gently via pipette again and incubated on ice for a further 30 minutes, for a total of one hour incubation. Cells were pelleted using a plate spinner (5 minutes, 1200 \times g), then resuspended and pelleted twice in ice-cold assay media.

Finally, cells were resuspended in assay media containing the live/dead stain propidium iodide (Biotium, Catalog number 40017, final concentration 1 μ g/mL) and analyzed by flow cytometry.

For studies with variable concentrations of D-MoDE-A, the mean fluorescent intensity was collected for the cell population. An aliquot of cells that was treated with α -DNP (final concentration of 100 nM), but not D-MoDE-A, was used as a control to subtract cellular autofluorescence and non-D-MoDE-A mediated antibody binding to cells. For experiments with inhibitory molecules, D-MoDE-A was present at a final concentration of 40 nM. Inhibitors were added as either 100x solutions in PBS (DNP-OH3 and GalNAc) or as 10x solutions in PBS (ASOR, ORM, ASF, and fetuin). Inhibitors were added after adding antibodies to cells, but before adding D-MoDE-A. To account for intraassay variability, the percent ternary complex formed was calculated by comparing against positive (cells, antibody, and compound) and negative (cells and antibody only) controls included in each assay.

Endocytosis assays

HepG2 cells were grown to confluency in a 96 well plate and washed with PBS. Cells were treated with premixed D-MoDE-A (40 nM final concentration) and AF488-labeled α -DNP (100 nM final concentration) at 37 °C in an incubator for six hours unless otherwise noted. In assays including competitive binders of ASGPR or α -DNP, inhibitors were added as 100x or 10x solutions as described above. Inhibitors were added to the antibody/compound mixture before adding the mixture to cells. Concentrations were chosen which were previously observed to reduce ternary complex formation by more than 90%.

In the case of experiments which utilized chemical inhibitors of endocytosis, compounds were added as 100x stocks in DMSO to antibody-compound mixtures before addition to cells. After 6 hours, media was aspirated and cells were washed with PBS, then removed from the plate by treatment with trypsin at 37 °C for 5 minutes. Cells were then treated with assay media containing propidium iodide and examined by flow cytometry. The control conditions were also treated with 1% DMSO as a vehicle control.

Microscopy studies

Cells were grown in 8-well microscope cell culture containers (Thermo, 177402) treated with polylysine (Fisher Scientific, 343810001). For all experiments, D-MoDE-A was used at a final concentration of 40 nM, and antibody was used at a final concentration of 100 nM. At 12 hours, cell culture media was removed and cells were washed with PBS once before fixation with 3.5% formaldehyde PBS solution for 13 minutes. Cells were then washed with PBS, and permeabilized for 5 minutes with 0.5% triton X-100 in PBS. Cells were blocked with 0.2% tween in TBS (Tween 20, AmericanBio, Ref AB02038-00500) and 3% BSA (Sigma, A9418) for one hour at room temperature. Primary antibodies (EEA1, Abcam ab70521; Lamp2, Abcam ab25631) were diluted as suggested by the manufacturer into 0.2% TBST + 3% BSA. After incubation for 1 hour in a humidified chamber protected from light, cells were washed 3x with PBST for 5 minutes each. Cells were then treated with Alexa Fluor 568-labeled secondary antibody (Abcam, ab175473) at 1:500 dilution. Cells were washed 3x with PBST for 5 minutes each, then treated with PBS containing Hoechst stain (final concentration 1 μ g/mL), incubated at room temperature for at least 10 minutes, and imaged. Cells were visualized using a Zeiss Axio Observer Z1 inverted microscope using 63x magnification under oil. Image analysis was performed on ZEN2 (blue edition) version 2.0.0.0.

In vitro degradation assay

Cells were grown in 24-well plates, and washed gently with PBS before adding antibody and D-MoDE-A. Compound (at 40 nM final concentration) and antibody (at 100 nM final concentration) where applicable were premixed and added to cells. At the given time point, cell culture media was collected and cells were washed 4x with PBS for 5 minutes each. Cells were then treated with PBS with 1x RIPA buffer (Millipore-Sigma, 20-188) with protease inhibitor tablets containing EDTA (Sigma, 11697498001) (50 μ L per well). Cells were incubated on ice for 5 minutes, after which each well was thoroughly washed with pipette and collected. Lysates were briefly centrifuged before taking supernatant samples for gel analysis to avoid aspirating the cell pellet. 5 μ L of each cell lysate was added per lane. For supernatants, 0.2 μ L of the supernatant was added for each lane.

For western blots, samples were diluted into Laemeli buffer containing SDS but not β -mercaptoethanol. Samples were boiled for 2 minutes in PCR tubes using an S1000 thermal cycler. Samples were then loaded onto anyKd gels (Bio-rad, 4569033) and run at 120V using a BIORAD mini-protean tetra system with a BIORAD power pack. Gels were then transferred to 0.45 μ m Immobilon-P PVDF membranes (Immobilon, Cat. No. IPVH00010) using 300 mA for 1 hour at 4 °C in transfer buffer (20% MeOH, 25 mM tris base, 192 mM glycine). Membranes were then blocked with 0.2 μ m-filtered 5% BSA in PBS for 1 hour. Anti-AF488 polyclonal antibody (Thermo, A-11094) diluted 1:10,000 into PBS containing 5% BSA was then added and the blots rocked gently for 1 hour. The membranes were then washed three times with PBS containing 0.2% Tween 20 (AmericanBio, Ref AB02038-00500) for 5 minutes each, then probed with HRP-conjugated goat α -rabbit antibody (1:10,000 in PBS containing 5% BSA, Abcam, ab205718). The membranes were gently rocked for 1 hour at room temperature, then washed 3 times with PBST for 5 minutes each and imaged. In the case of actin, we utilized an α -actin mouse antibody (Abcam, ab8226) followed by goat α -mouse HRP conjugate (Abcam, ab205719). Gels were imaged using a BIO-RAD ChemiDoc touch imaging system.

In vivo assays

In vivo experiments were performed under IUCAC supervision following protocol entitled “pre-clinical evaluation of small molecule immunomodulators” (Protocol number 2017-11445; Approval date August 30 2017; Expiration July 31 2020). Experiments were performed in male nude mice purchased from Jackson Laboratory (NU/J, Stock No. 002019). Compounds were administered i.p. in a volume of 100 μ L PBS. Approximately 25 μ L of blood was collected at each time point by saphenous bleed. Antibody was administered as 200 μ g in 100 μ L i.p. In the case of experiments where 500 μ g IgG was injected, the antibody was administered in a volume of 250 μ L i.p. For experiments in which twice daily dosing regimes were followed, the second dose was given six hours after the first. Unless otherwise noted, compounds were administered daily at the specified dose throughout the course of experiments. For data analysis, antibody levels were normalized to the highest recorded concentration of antibody observed in each mouse, which was generally 24 hours after the i.p. administration of antibody.

Mouse monoclonal α -DNP production

Antibodies were produced in U7.6 hybridoma cell lines donated by the Eshhar Lab at the Weizmann Institute. Purification and cell culture were carried out according to published methods (47). Cells were thawed and culture in 75 cm² flasks (Corning, 353136) using high glucose DMEM containing pyruvate and L-glutamine (Invitrogen, 11995-065) supplemented with 15% Horse

Serum (Invitrogen, 16050-114) and Pen strep (Invitrogen, 10378-016). Cells were passaged every 3 days until greater than 90% of the cells were viable. They were then transferred to CELLLine1000 Bioreactors (VWR, 37003-008) through inoculation with approximately 75×10^6 cells. They were grown in the cell compartment in DMEM containing 15% IgG Depleted FBS (Invitrogen, 16250-078) and Pen/Strep. Nutrient compartment contained compartment media (DMEM supplemented with 5% horse serum and Pen/Strep). Cells were incubated for 5 days at 37 °C in a 5% CO₂ atmosphere.

When cells reached $20\text{-}30 \times 10^6$ cells/mL, they were pelleted ($300 \times g$ for 10 minutes) and the supernatant collected. Supernatant containing α -DNP IgG2a was clarified by filtration through a 0.22 micron sterile filter, then stored at -80 °C. IgG was purified using 5 mL protein G spin columns (Thermo, 89961). Purity was confirmed using SDS-PAGE. Activity and isotype were confirmed using sandwich ELISA performed with DNP-modified BSA and an α -mouse IgG2a antibody (Novus Biologicals, 7511).

Mouse polyclonal α -DNP production

Mouse polyclonal serum was prepared by immunization of male C57BL/6 mice (Jackson Laboratory, stock no. 000664). Appropriately aged male mice (>6 weeks old) were chosen. DNP-KLH was suspended in sterile PBS to 2 mg/mL (2x solution). This was diluted 1:1 with Complete Freund's Adjuvant (from EMD Millipore) and vortexed to achieve a smooth suspension. For booster doses, Freund's incomplete adjuvant (iCFA) (from EMD Millipore) was used. For all doses, 100 μ L was injected i.p. into mice. Two weeks post-immunization, mice were boosted by another injection of antigen. Following that, mice were boosted every week (up to five times) until the concentration of α -DNP was between 0.5 and 1.0 mg/mL, at which time serum was collected. Serum was pooled and injected into mice at a volume of 200 μ L.

ELISA to measure serum levels of α -DNP

ELISA analysis of serum samples was performed using MaxiSorp 96 well plates (Thermo, 44-2404-21). Plates were coated with 50 μ L of BSA-DNP (Invitrogen, A23018) at 100 μ g/mL in PBS and incubated at 4 °C overnight. Coating solution was then removed, and the plates were blocked with 2% BSA in PBS for 2 hours at room temperature, followed by washing twice with PBST (.2% Tween). Serum samples were diluted in 2% BSA in PBS. For samples collected on days 1-4, serum was diluted 1:5,000. For day 5 and after, serum was diluted 1:1,000 to account for lower levels of circulating antibody present in serum. Diluted samples were added to the plate for 1 hour at RT. Plates were then washed with PBST (3 times), followed by addition of goat α -mouse IgG-HRP conjugate (Ab 97265) diluted in 2% BSA in PBS (1:10,000). The plates were incubated for 1 hour at RT, then washed three times with PBST. The plates were then treated with TMB (Thermo 34028) followed by 2 M H₂SO₄ and analyzed for OD at 450 nm on a plate reader (BioTek Synergy 2). Sample concentrations were determined against a standard curve.

AST/ALT measurement

AST and ALT levels were determined using pooled serum from mice from the study in Figure 4C. Samples were submitted to the Mouse Metabolic Phenotyping Center at the Yale Diabetes Research Center.

Half life determination

Half life, AUC, and bioavailability were measured by Aurigene Discovery Technologies Ltd. Male nude mice were injected with 1mpk dose i.p. in 200 μ L 5% DMSO, 30% PEG300, and 65% water. Blood samples were collected (sub-mandibular) and the concentration of D-MoDE-A was measured by LC-MS/MS. Time points were 0, 5, 15, and 30 minutes, and 1, 2, 3, 6, 12, and 24 hours.

Synthetic methods

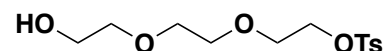
General chemistry methods

Flash chromatography was performed on a CombiFlash NEXTGEN 300+ system by Teledyne ISCO running software version 5.0.62. Separation was accomplished on RediSep Rf High performance gold C18 columns (reverse phase) and RediSep Rf flash columns (normal phase). HPLC purification of compounds was performed using a Shimadzu chromatography system using a Waters SunFire C18 OBD Prep Column (10 mm x 150 mm) and the LabSolutions Software Version 5.92. NMR analysis was performed on Agilent DD2 400 MHz and Agilent DD2 600 MHz NMR spectrometers. The 600 MHz instrument was equipped with a C[H] cold probe. HRMS analysis was performed on a Shimadzu 9030 Quadrupole Time-of-Flight LC-MS system following separation on a Shim-pack Scepter C18-120 1.9 μm (2.1 x 50 mm) reverse phase chromatography column. Separation was performed using a gradient of water to acetonitrile with the addition of 0.1% formic acid. Infrared (IR) spectra were collected using neat samples and recorded using a Thermo Nicolet 6700 equipped with a diamond ATR cell. Select ν_{ma} are reported in cm^{-1} . Optical rotation was recorded on a Rudolph Autopol IV polarimeter. Chemicals were purchased from Sigma Aldrich, Fisher, and Carbosynth. Solvents were purchased from Fisher and Macron.

Synthetic methods

Compound 1 (48)

2-(2-(2-hydroxyethoxy)ethoxy)ethyl 4-methylbenzenesulfonate



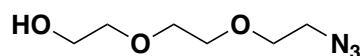
Triethylene glycol (17.5 mL, 19.7 g, 131 mmol, 5 eq) was dissolved in dichloromethane (150 mL) and triethylamine (5.48 mL, 3.98 g, 1.5 eq) and cooled to 0 °C. *p*-Toluenesulfonyl chloride (5.00 g, 26.2 mmol, 1.00 eq) was then added and the reaction mixture stirred at room temperature for 18 hours. The reaction was then diluted into dichloromethane and washed with water (3x) and brine (1x). The organic layer was dried over sodium sulfate and concentrated *in vacuo* to give compound **1** (6.89 g, 22.6 mmol) as a pale yellow oil in 85% yield, which was used without further purification. Spectra matched previously reported characterization data.

^1H NMR (400 MHz, Chloroform-*d*): δ 7.80 (d, J = 8.3 Hz, 2H), 7.38 – 7.30 (m, 2H), 4.23 – 4.14 (m, 2H), 3.71 (td, J = 5.3, 4.3 Hz, 4H), 3.66 – 3.55 (m, 6H), 2.45 (s, 3H).

^{13}C NMR (101 MHz, Chloroform-*d*): δ 144.98, 133.09, 129.95, 128.09, 72.58, 70.91, 70.44, 69.28, 68.84, 61.88, 21.76.

Compound 2 (48)

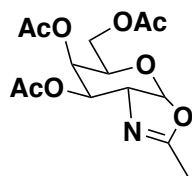
2-(2-(2-azidoethoxy)ethoxy)ethan-1-ol



Tosylate **1** (2.00 g, 6.57 mmol) and sodium azide (0.470 g, 7.23 mmol, 1.1 eq) were dissolved in dimethylformamide (40 mL) and stirred overnight at 60 °C. Volume was reduced by approx. half by rotary evaporation at 70 °C, and the resulting mixture was diluted into water and extracted with ethyl acetate (2x). The combined organic layers were washed with brine (3x), dried over sodium sulfate, and evaporated to give azide **2** as a colorless oil (932 mg, 5.32 mmol) in 81% yield, which was used without further purification.

Compound 3 (49)

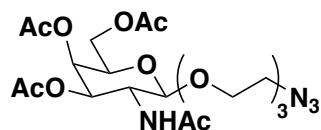
(5*R*,6*R*,7*R*,7*aR*)-5-(acetoxymethyl)-2-methyl-3*a*,6,7,7*a*-tetrahydro-5*H*-pyrano[3,2-*d*]oxazole-6,7-diyl diacetate



D-Galactosamine pentaacetate (100 mg, 0.257 mmol) was dissolved in dichloroethane (1.0 mL) and stirred at room temperature under nitrogen atmosphere before the addition of trimethylsilyl trifluoromethanesulfonate (70.0 μ L, 86.0 mg, 0.387 mmol, 1.50 eq). The reaction was stirred at 50 °C for 90 minutes, then allowed to cool to room temperature and stirred for a further 12 hours. The reaction was then poured into ice cold saturated aqueous sodium bicarbonate and extracted into dichloromethane. The organic layer was washed with water (2x) then dried over sodium sulfate and evaporated to give compound **3** (236 mg, 77.7 μ mol, 92%) as a dark gum, which was used without further purification.

Compound 4 (50)

(2*R*,3*R*,4*R*,5*R*,6*R*)-5-acetamido-2-(acetoxymethyl)-6-(2-(2-(2-azidoethoxy)ethoxy)ethoxy)tetrahydro-2*H*-pyran-3,4-diyl diacetate



Compound **3** (200 mg, 0.607 mmol) and compound **2** (160 mg, 0.913 mmol, 1.50 eq) were dissolved in 1,2-dichloroethane (5 mL). 4 Å molecular sieves were then added, and the reaction stirred for 30 minutes. Trimethylsilyl trifluoromethanesulfonate (55.0 μ L, 67.5 mg, 0.304 mmol, 0.5 eq) was then added to the mixture, and the reaction stirred overnight. The reaction was then diluted into dichloromethane, washed with 1 M sodium bicarbonate (1x) and water (1x), then dried over magnesium sulfate and concentrated. The crude oil was purified on silica gel (50-100% ethyl

acetate in dichloromethane) to give compound **4** (245 mg, 0.486 mmol) as a white solid in 80.1% yield. Spectra matched previously reported characterization data.

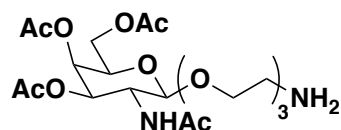
^1H NMR (400 MHz, Chloroform-*d*) δ 6.13 (d, J = 9.3 Hz, 1H), 5.31 (dd, J = 3.4, 1.1 Hz, 1H), 5.05 (dd, J = 11.2, 3.4 Hz, 1H), 4.77 (d, J = 8.6 Hz, 1H), 4.28 – 4.04 (m, 3H), 3.93 – 3.79 (m, 3H), 3.78 – 3.58 (m, 8H), 3.43 (dt, J = 28.2, 4.9 Hz, 4H), 2.15 (s, 3H), 2.04 (s, 3H), 1.98 (s, 3H), 1.97 (s, 3H).

^{13}C NMR (101 MHz, Chloroform-*d*) δ 170.24, 170.09, 169.99, 101.84, 72.06, 71.27, 70.50, 70.29, 70.27, 70.20, 70.00, 69.98, 69.67, 69.37, 68.18, 66.30, 61.38, 61.17, 50.32, 50.26, 50.11, 22.80, 20.37, 20.31.

HRMS: $[\text{M}+\text{Na}]^+$ Expected 527.207 Found 527.206

Compound 5 (50)

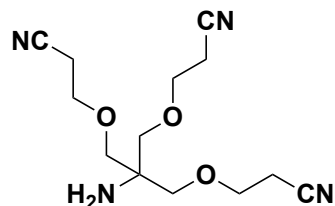
(2*R*,3*R*,4*R*,5*R*,6*R*)-5-acetamido-2-(acetoxymethyl)-6-(2-(2-(2-aminoethoxy)ethoxy)ethoxy)tetrahydro-2*H*-pyran-3,4-diyl diacetate



Compound **4** (1.80 g, 3.57 mmol) was dissolved in tetrahydrofuran (35 mL). Triphenylphosphine (1.40 g, 5.35 mmol, 1.5 eq) and water (257 μL , 14.28 mmol, 4 eq) were then added and the reaction stirred at room temperature under nitrogen for 36 hours. The solvent was removed and the crude product, a colorless oil, was used in the next step without further purification.

Compound 6 (51)

3,3'-((2-amino-2-((2-cyanoethoxy)methyl)propane-1,3-diyl)bis(oxy))dipropanenitrile



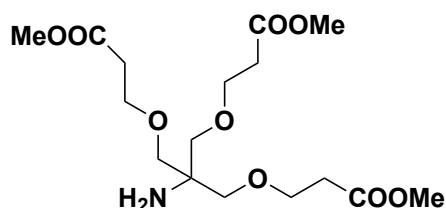
Tris(hydroxymethyl)aminomethane (1.00 g, 8.25 mmol, 1.00 eq) was dissolved in dioxane (50 mL) and aqueous KOH (40% w/v, 1 mL) was added dropwise. Acrylonitrile (6.45 mL, 5.22 g, 25.2 mmol, 3.05 eq) was then added dropwise, and the reaction stirred overnight. Dioxane was removed *in vacuo* and the resulting aqueous solution was extracted with dichloromethane (3x). The combined organic layers were then washed with brine (1x), dried over sodium sulfate, and evaporated to give compound **6** as a colorless oil (1.12 g, 4.04 mmol) in 48.5% yield, which was used in further steps without purification. Spectra matched previously reported characterization data.

^1H NMR (600 MHz, Chloroform-*d*) δ 3.70 (t, J = 6.0 Hz, 6H), 3.48 (s, 6H), 2.63 (t, J = 6.0 Hz, 6H).

^{13}C NMR (151 MHz, Chloroform-*d*) δ 118.01, 72.15, 65.75, 56.41, 18.86.

Compound 7 (52)

dimethyl 3,3'-((2-amino-2-((3-methoxy-3-oxopropoxy)methyl)propane-1,3-diyl)bis(oxy))dipropionate



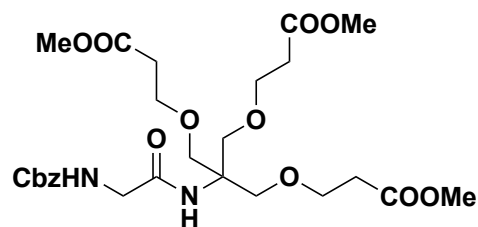
Compound **6** (710 mg, 2.50 mmol) was dissolved in methanol (30 mL) and sulfuric acid (2.8 mL) and heated at reflux for 24 hours. The solution was then cooled to 0 °C, then neutralized with saturated sodium bicarbonate solution, and extracted into dichloromethane (3x). The organic layer was washed with brine, then dried over sodium sulfate and concentrated. The residue was purified on silica gel (0-10% methanol in dichloromethane) to give compound **7** as a colorless oil (656 mg, 1.73 mmol) in 69.0% yield. Spectra matched previously reported characterization data.

^1H NMR (400 MHz, Chloroform-*d*) δ 3.71-3.68 (m, 6H), 3.69 (s, 9H), 3.33 (s, 6H), 2.56 (t, J = 6.3 Hz, 6H).

^{13}C NMR (101 MHz, Chloroform-*d*) δ 172.03, 72.41, 66.79, 56.23, 51.63, 34.80.

Compound 8

methyl 8,8-bis((3-methoxy-3-oxopropoxy)methyl)-3,6-dioxo-1-phenyl-2,10-dioxo-4,7-diazatriodecan-13-oate



Compound **7** (723 mg, 1.90 mmol) was dissolved in acetonitrile (25 mL). 1-hydroxybenzotriazole hydrate (291 mg, 1.90 mmol, 1 eq), N-carbobenzyloxyglycine (397 mg, 1.90 mmol, 1.00 eq), and N,N'-dicyclohexylcarbodiimide (392 mg, 1.90 mmol, 1.00 eq) were then added, and the reaction stirred overnight. Acetonitrile was then evaporated, and the residue adsorbed onto silica and

purified using a gradient of 0-75% ethyl acetate in hexanes. Compound **8** (866 mg, 1.52 mmol) was recovered as a colorless oil in 80% yield.

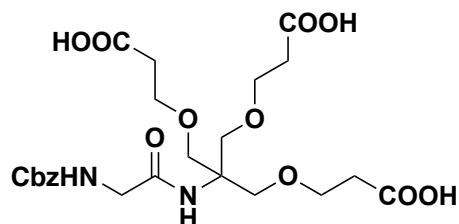
^1H NMR (600 MHz, Chloroform-*d*) δ 7.33 (dd, J = 24.9, 4.4 Hz, 5H), 6.33 (s, 1H), 5.55 (s, 1H), 5.12 (s, 2H), 3.86 (d, J = 5.1 Hz, 2H), 3.68 (t, J = 5.5 Hz, 21H), 2.53 (t, J = 6.1 Hz, 6H)

^{13}C NMR (151 MHz, Chloroform-*d*) δ 172.14, 168.67, 156.32, 136.41, 128.45, 128.05, 127.98, 69.04, 66.85, 66.71, 59.83, 51.69, 44.55, 34.64.

HRMS: $[\text{M}+\text{H}]^+$ Expected 571.250, Found 571.243

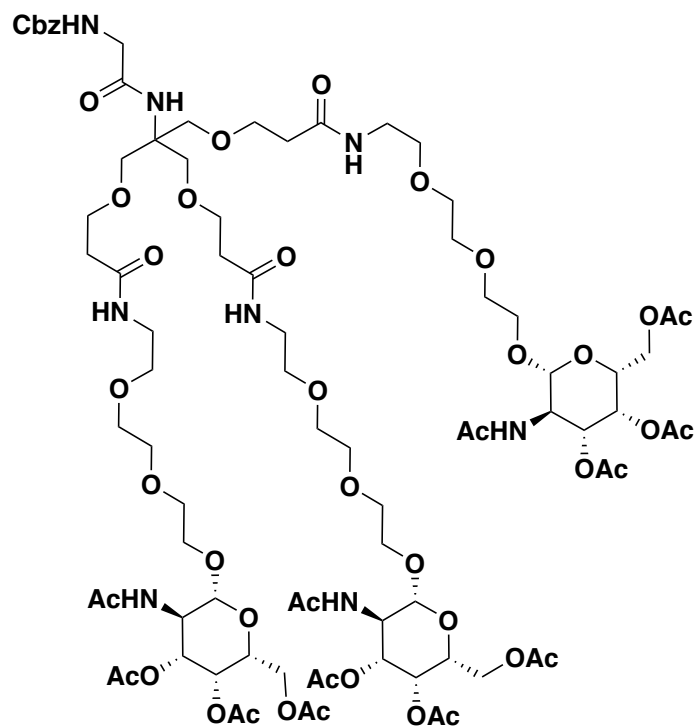
Compound 9

8,8-bis((2-carboxyethoxy)methyl)-3,6-dioxo-1-phenyl-2,10-dioxo-4,7-diazatridecan-13-oic acid



Compound **8** (100 mg, 0.175 mmol) was dissolved in dioxane (2 mL) and aqueous NaOH (2 M, 2 mL). The reaction was stirred for 3 hours, then acidified to approximately pH 3 with 6 M hydrochloric acid and extracted twice into ethyl acetate. The organic fraction was washed with 1 M HCl, then dried over sodium sulfate and evaporated to give compound **9** as a white solid, which was used in further steps without purification.

Compound 10



Compound **9** (372 mg, 0.704 mmol, 1 eq) was dissolved in dimethylformamide (40 mL) and diisopropylethylamine (981 μ L, 728 mg, 5.63 mmol, 8.00 eq). N,N,N',N'-Tetramethyl-O-(1H-benzotriazol-1-yl)uronium hexafluorophosphate (HBTU) (1.01 g, 2.67 mmol, 3.8 eq) was then added, and the reaction stirred for 10 minutes at room temperature before the addition of compound **5** (1.28 g, 2.67 mmol, 3.8 eq). The reaction was stirred for two hours, then diluted into dichloromethane and washed with aqueous solutions of phosphoric acid (1 M, 1x), sodium bicarbonate (1 M, 1x), and brine (1x). The organic layer was dried over sodium sulfate and evaporated onto silica. The residue was purified (0-20% methanol in dichloromethane) to give compound **10** (831 mg, 0.436 mmol) as a light brown solid in 62% yield.

^1H NMR (500 MHz, DMSO- d_6) δ 7.91 (t, J = 5.7 Hz, 3H), 7.80 (d, J = 9.2 Hz, 3H), 7.39 - 7.28 (m, 6H), 7.12 (s, 1H), 5.21 (d, J = 3.4 Hz, 3H), 5.02 (s, 2H), 4.97 (dd, J = 11.2, 3.4 Hz, 3H), 4.55 (d, J = 8.5 Hz, 3H), 4.10 - 3.99 (m, 9H), 3.92 - 3.84 (m, 3H), 3.81 - 3.75 (m, 3H), 3.62 - 3.46 (m, 35H), 3.39 (t, J = 6.1 Hz, 6H), 3.23 - 3.16 (m, 6H), 2.30 (t, J = 6.4 Hz, 6H), 2.10 (s, 9H), 1.99 (s, 9H), 1.89 (s, 9H), 1.77 (s, 9H).

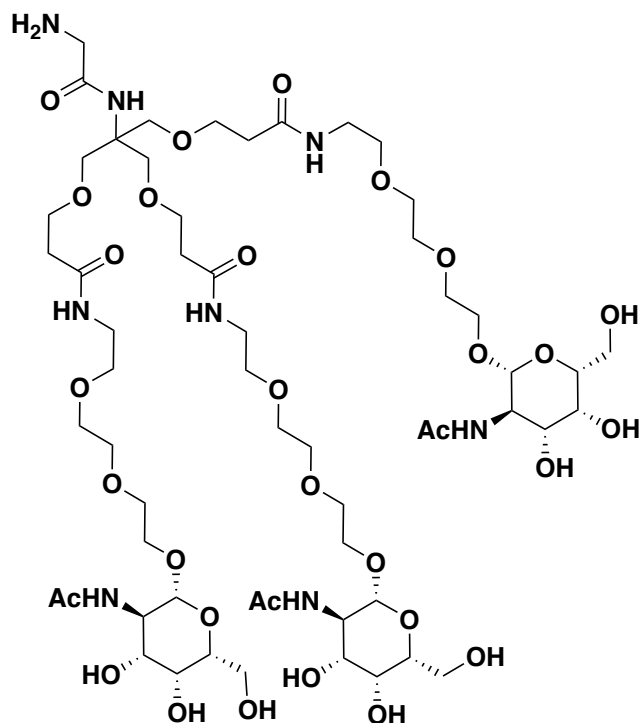
^{13}C NMR (126 MHz, DMSO- d_6) δ 170.40, 170.16, 170.09, 169.79, 169.48, 169.04, 156.60, 137.23, 128.50, 127.94, 127.84, 101.12, 72.50, 70.65, 70.07, 69.93, 69.86, 69.77, 69.59, 69.29, 68.50, 67.51, 66.89, 65.59, 61.63, 60.38, 59.84, 49.50, 43.77, 38.68, 36.01, 22.95, 20.68, 20.62, 20.60.

HRMS: $[\text{M}+\text{Na}]^+$ Expected 1931.802, Found 1931.802

$[\alpha]_D = -13.82^\circ$ (c = 1 g/100 mL, MeOH, 24.13 $^\circ\text{C}$)

IR $f(\text{cm}^{-1})$: 3300, 2929, 2873, 1645, 1552, 1373, 1247, 1053, 590

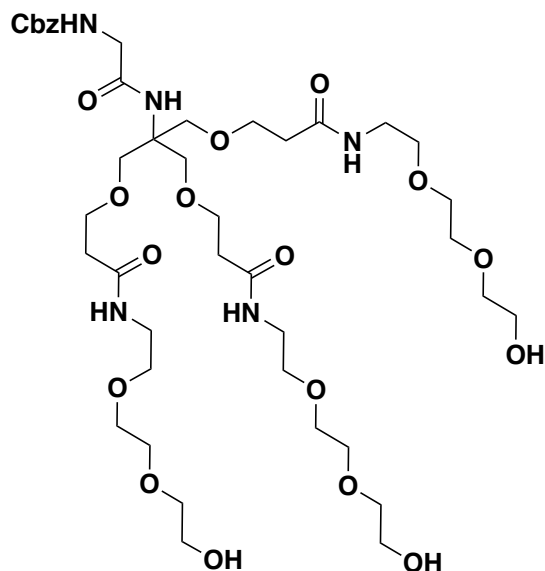
Compound 11



Compound **10** (710 mg, 0.372 mmol) was dissolved in dry methanol (90 mL) and cooled to 0 °C under nitrogen. Palladium on carbon (71.0 mg, 10% w/w) was then added, and the reaction stirred under hydrogen atmosphere (1 atm) at 0 °C for 16 hours. Upon completion, the reaction was filtered through celite and methanol was evaporated to give the intermediate amine (657 mg, 0.370 mmol) in 99.5% yield, which was used without further purification. The amine (441 mg, 0.248 mmol) was dissolved in methanol (15 mL) and cooled to 0 °C. Sodium methoxide solution (400 μ L, 5.4M in MeOH) was then added to effect removal of the *O*-acetyl groups, and the reaction was stirred for 30 minutes. Dowex 50WX8 was then added until the solution was weakly acidic. The resin was filtered and washed thoroughly with methanol. The combined methanol fractions were evaporated under reduced pressure to give compound **11** (274 mg, 0.196 mmol) as a colorless oil in 79.0% yield. Compound **11** was used in further steps without purification.

Compound 12

benzyl (1-hydroxy-15,15-bis(14-hydroxy-5-oxo-2,9,12-trioxa-6-azatetradecyl)-10,17-dioxo-3,6,13-trioxa-9,16-diazaoctadecan-18-yl)carbamate



Compound **9** (302 mg, 0.572 mmol, 1 eq) was dissolved in dichloromethane (25 mL) and triethylamine (480 μ L, 3.431 mmol, 6.00 eq). 1-Hydroxybenzotriazole hydrate (350 mg, 2.28 mmol, 4 eq) and 1-ethyl-3-(3-dimethylaminopropyl)carbodiimide (417 mg, 2.17 mmol, 3.80 eq) were then added, followed by 2-[2-(2-Aminoethoxy)ethoxy]ethanol (300 mg, 2.01 mmol, 3.80 eq). The reaction was then stirred overnight. The solvent was evaporated and the crude material was purified by reverse phase chromatography without workup using a gradient of 5-35% acetonitrile in water with the addition of 0.1% formic acid. Compound **12** was recovered in 65% yield as a colorless oil (345 mg, 0.372 mmol).

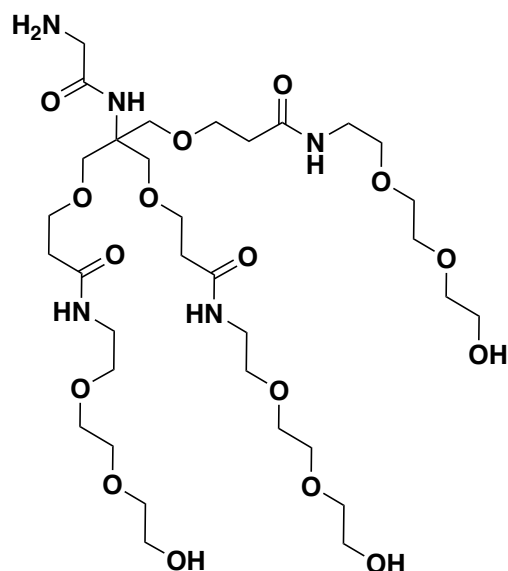
^1H NMR (500 MHz, DMSO- d_6) δ 7.90 (t, J = 5.6 Hz, 3H), 7.35 (q, J = 7.1 Hz, 6H), 7.11 (s, 1H), 5.03 (s, 2H), 4.57 (t, J = 5.4 Hz, 3H), 3.65 – 3.45 (m, 30H), 3.40 (q, J = 6.3, 5.8 Hz, 12H), 3.19 (p, J = 7.1, 6.5 Hz, 6H), 2.30 (t, J = 6.5 Hz, 6H).

^{13}C NMR (151 MHz, DMSO- d_6) δ 170.24, 168.88, 156.44, 137.07, 128.35, 127.79, 127.70, 72.34, 69.69, 69.61, 69.12, 68.31, 67.35, 65.43, 60.21, 59.68, 43.57, 38.53, 35.85.

HRMS: $[\text{M}+\text{H}]^+$ Expected 922.4872, Found 922.4894

Compound 13

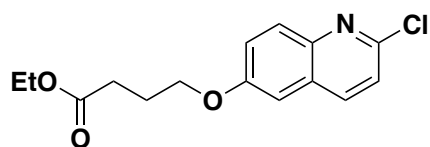
3,3'-((2-(2-aminoacetamido)-2-(14-hydroxy-5-oxo-2,9,12-trioxa-6-azatetradecyl)propane-1,3-diyl)bis(oxy))bis(*N*-(2-(2-(2-hydroxyethoxy)ethoxy)ethyl)propanamide)



Compound **12** (345 mg, 0.374 mmol, 1.00 eq) was dissolved in methanol (15 mL). The solution was purged under a stream of nitrogen for five minutes. 10% Pd/C (5% w/w, 17.3 mg) was then added under a stream of nitrogen. The mixture was purged with hydrogen gas for 5 minutes and then stirred for 2 hours under a hydrogen atmosphere. The mixture was then filtered through a bed of celite and the filtrate concentrated *in vacuo* to give compound **13** as a colorless oil in 96% yield (282 mg, 0.359 mmol). Compound **13** was used in further steps without purification.

Compound 14 (53)

ethyl 4-((2-chloroquinolin-6-yl)oxy)butanoate



2-chloroquinolin-6-ol (1.00 g, 5.57 mmol) and potassium carbonate (1.53 g, 11.1 mmol, 2.0 eq) were dissolved in dimethylformamide (20 mL). Ethyl bromobutyrate (1.63 g, 1.2 mL, 8.35 mmol, 1.5 eq) was then added and the mixture stirred at 80 °C for 12 hours. The reaction was diluted into ethyl acetate and washed with water (2x) and brine (3x). The organic layer was dried over sodium sulfate and evaporated to give compound **14** as a pale yellow solid, which was used in the next step without further purification. Spectra matched previously reported characterization data.

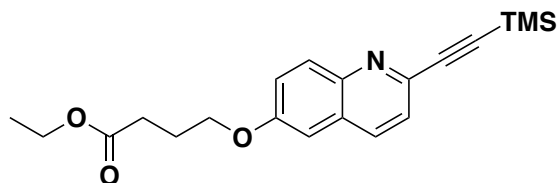
¹H NMR (400 MHz, Chloroform-*d*) δ 7.98 (d, *J* = 8.6 Hz, 1H), 7.92 (d, *J* = 9.2 Hz, 1H), 7.40 – 7.32 (m, 2H), 7.07 (d, *J* = 2.7 Hz, 1H), 4.20 – 4.09 (m, 5H), 2.56 (t, *J* = 7.2 Hz, 2H), 2.19 (t, *J* = 6.7 Hz, 2H), 1.26 (t, *J* = 7.1 Hz, 4H).

¹³C NMR (101 MHz, Chloroform-*d*) δ 173.24, 157.46, 148.18, 143.87, 137.83, 130.05, 128.06, 123.40, 122.67, 106.20, 77.48, 77.16, 76.84, 67.30, 60.69, 30.87, 24.63, 14.39.

HRMS: $[M+H]^+$ Expected 294.0897, Found 294.0912

Compound 15 (53)

ethyl 4-((2-((trimethylsilyl)ethynyl)quinolin-6-yl)oxy)butanoate



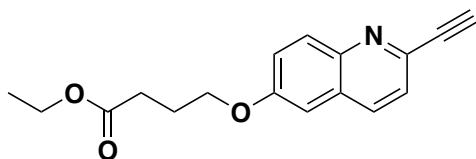
Compound **14** (1.52 g, 5.17 mmol) was dissolved in tetrahydrofuran (20 mL) and triethylamine (2.88 mL, 20.7 mmol, 4 eq). Copper (I) iodide (49.0 mg, 0.258 mmol, 0.050 eq), Bis(triphenylphosphine)palladium(II) dichloride (181 mg, 0.258 mmol, 0.050 eq), and trimethylsilylacetylene (1.07 mL, 762 mg, 7.75 mmol, 1.50 eq) were then added and the reaction was stirred in a pressurized vessel at 65 °C for 16 hours. The reaction mixture was then cooled and filtered through celite. The celite was washed extensively with ethyl acetate, and the combined organic fractions were evaporated. The residue was purified on silica (0-50% ethyl acetate in hexanes) to give compound **15** in 81% yield (1.49 g, 4.19 mmol) as a pale yellow solid. Spectra matched previously reported characterization data.

^1H NMR (500 MHz, Chloroform-*d*) δ 8.00 (d, J = 8.4 Hz, 2H), 7.50 (d, J = 8.5 Hz, 1H), 7.43 – 7.33 (m, 1H), 7.04 (d, J = 2.2 Hz, 1H), 4.15 (dt, J = 12.7, 6.5 Hz, 4H), 2.56 (t, J = 7.2 Hz, 2H), 2.24 – 2.13 (m, 2H), 1.26 (t, J = 7.1 Hz, 3H), 0.30 (s, 9H).

^{13}C NMR (151 MHz, Chloroform-*d*) δ 173.07, 124.73, 105.65, 67.11, 60.51, 30.67, 24.42, 14.21, -0.27.

Compound 16 (53)

ethyl 4-((2-ethynylquinolin-6-yl)oxy)butanoate



Compound **15** (1.57 g, 4.42 mmol) was dissolved in dichloromethane (45 mL) and tetrabutylammonium fluoride (5.30 mL, 1.00 M in THF, 5.30 mmol, 1.20 eq) was added dropwise. After 1 minute of stirring, 10% citric acid (50 mL) was added and the reaction stirred for 30 minutes. The organic phase was washed with water (1x), dried, and evaporated to give compound **16** as a pale yellow solid, which was used in the next step without further purification. Spectra matched previously reported characterization data.

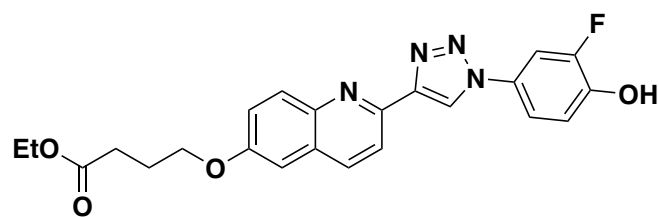
^1H NMR (600 MHz, Chloroform-*d*) δ 8.11 – 8.00 (m, 1H), 7.51 (d, J = 8.4 Hz, 1H), 7.38 (dd, J = 9.3, 2.3 Hz, 1H), 7.05 (d, J = 2.4 Hz, 1H), 4.15 (p, J = 6.6, 6.0 Hz, 3H), 3.43 – 3.36 (m, 1H), 2.56 (t, J = 7.2 Hz, 1H), 2.22 – 2.14 (m, 1H), 1.73 – 1.64 (m, 1H), 1.47 (q, J = 7.4 Hz, 1H), 1.26 (t, J = 7.1 Hz, 2H), 1.02 (t, J = 7.3 Hz, 1H).

^{13}C NMR (151 MHz, Chloroform-*d*) δ 173.06, 137.60, 129.91, 128.64, 124.50, 123.18, 122.48, 105.99, 105.58, 77.20, 76.99, 76.77, 67.12, 60.51, 59.14, 30.67, 24.42, 24.22, 19.80, 14.21, 13.69.

HRMS: $[\text{M}+\text{H}]^+$ Expected 284.1287, Found 284.1285

Compound 17 (53)

ethyl 4-((2-(1-(3-fluoro-4-hydroxyphenyl)-1*H*-1,2,3-triazol-4-yl)quinolin-6-yl)oxy)butanoate



2-fluoro-4-iodophenol (126 mg, 0.529 mmol) and sodium azide (38 mg, 0.528 mmol, 1.0 eq) were dissolved in DMSO (2.5 mL) and stirred for 2 hours at 70 °C. Compound 32 (150 mg, 0.529 mmol, 1 eq), trans-*N,N'*-dimethylcyclohexane-1,2-diamine (11 mg, 0.079 mmol, 0.15 eq), sodium ascorbate (10 mg, 0.053 mmol, 0.1 eq), copper (I) iodide (15 mg, 0.079 mmol, 0.15 eq), and H_2O (2.5 mL) were then added, and the mixture stirred at 70 °C overnight. The reaction was diluted with ethyl acetate and washed with water (1x) and brine (1x). The organic layer was dried over sodium sulfate, evaporated, and purified on silica (0-100% ethyl acetate in dichloromethane) to give compound **17** as an off-white solid. Spectra matched previously reported characterization data.

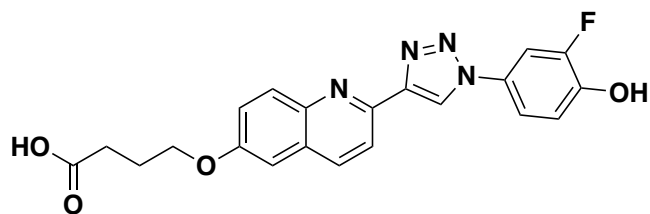
^1H NMR (600 MHz, DMSO-*d*₆) δ 10.46 (s, 1H), 9.32 (s, 1H), 8.39 (d, J = 8.6 Hz, 1H), 8.23 (d, J = 8.5 Hz, 1H), 7.95 (dd, J = 11.6, 2.6 Hz, 2H), 7.77 – 7.71 (m, 1H), 7.43 (dd, J = 4.8, 2.0 Hz, 2H), 7.16 (t, J = 9.0 Hz, 1H), 4.17 (d, J = 6.3 Hz, 2H), 4.13 – 4.07 (m, 3H), 3.17 (d, J = 5.2 Hz, 3H), 2.53 (d, J = 7.3 Hz, 3H), 2.07 (t, J = 6.8 Hz, 2H), 1.19 (d, J = 7.1 Hz, 3H), 0.94 (d, J = 7.3 Hz, 1H).

^{13}C NMR (151 MHz, DMSO-*d*₆) δ 172.96, 156.95, 151.95, 150.34, 148.62, 145.98, 143.82, 136.47, 130.40, 129.01, 123.19, 121.83, 119.06, 118.62, 117.31, 109.87, 109.72, 107.12, 67.43, 60.35, 49.03, 40.48, 40.36, 40.22, 40.09, 39.95, 39.81, 39.67, 39.53, 30.61, 24.58, 23.48, 14.56, 13.93.

HRMS: $[\text{M}+\text{H}]^+$ Expected 437.163, Found 437.164

Compound 18 (53)

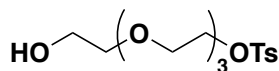
4-((2-(1-(3-fluoro-4-hydroxyphenyl)-1*H*-1,2,3-triazol-4-yl)quinolin-6-yl)oxy)butanoic acid



Compound **17** (90.0 mg, 0.206 mmol) was dissolved in dioxane (6.00 mL) and 2 M NaOH (3.00 mL). The reaction was stirred for 2.5 hours at room temperature, at which time the reaction was diluted with water and the pH adjusted to 3 with 1 M HCl. The mixture was cooled to 4 °C and filtered to give compound **18** as a brown powder, which was used without further purification.

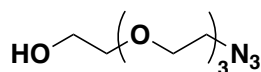
Compound 19 (54)

2-(2-(2-(2-hydroxyethoxy)ethoxy)ethoxy)ethyl 4-methylbenzenesulfonate



Tetraethylene glycol (50.0 g, 258 mmol) was dissolved in tetrahydrofuran (10 mL), cooled to 0 °C, and stirred. Sodium hydroxide (1.68 g, 41.3 mmol, 1.60 eq) in water (10 mL) was then added, followed by the dropwise addition of p-toluenesulfonyl chloride (5.00 g, 25.8 mmol, 1.00 eq) in tetrahydrofuran (3 mL). The reaction mixture was stirred at 0 °C for 4 hours, then diluted into dichloromethane. The organic layer was washed with ice-cold water (2x) and brine (1x), then dried over sodium sulfate to give compound **19** (8.84 g, 25.4 mmol, 99.0% yield) as a pale yellow oil, which was used in further steps without purification.

Compound 20 (54)



2-(2-(2-(2-azidoethoxy)ethoxy)ethoxy)ethan-1-ol

Compound **19** (8.84 g, 25.4 mmol) was dissolved in 100% ethanol (200 mL) and sodium azide (4.128 g, 63.5 mmol, 2.50 eq) was added. The reaction was heated to reflux for 16 hours, then cooled to room temperature before the addition of water (150 mL). Ethanol was then evaporated under reduced pressure and the aqueous layer extracted into ethyl acetate (2x). The organic layer was washed with water (1x) and brine (1x), dried over sodium sulfate, and evaporated to give compound **20** (4.82 g, 22.1 mmol) as a yellow oil in 87.0% yield. Spectra matched previously reported characterization data.

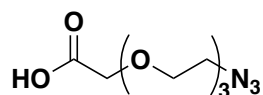
HNMR: ¹H NMR (400 MHz, Chloroform-*d*) δ 3.69 – 3.64 (m, 2H), 3.61 (m, *J* = 4.2 Hz, 10H), 3.57 – 3.51 (m, 2H), 3.33 (td, *J* = 5.0, 2.3 Hz, 2H), 2.81 (s, 1H).

CNMR: ^{13}C NMR (101 MHz, cdCl_3) δ 72.47, 70.65, 70.63, 70.59, 70.52, 70.28, 69.99, 61.60, 50.59.

HRMS: $[\text{M}+\text{H}]^+$ Expected 220.130, Found 220.128

Compound 21 (55)

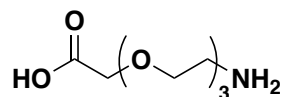
2-(2-(2-(2-azidoethoxy)ethoxy)ethoxy)acetic acid



Ice-cold Jones reagent was prepared separately by mixing chromium trioxide (1.37 g, 13.68 mmol, 3.00 eq), H_2SO_4 (2.38 mL), and water (26.2 mL) at 0 °C. Jones reagent was then added dropwise to an ice-cold solution of compound **20** (1.00 g, 4.56 mmol, 1 eq) in acetone (20 mL). The reaction was then warmed to room temperature and stirred for 16 hours. Excess Jones reagent was quenched by the addition of isopropanol (30 mL) and the reaction concentrated. The aqueous residue was then extracted with dichloromethane (4x). The organic layers were combined, dried over sodium sulfate, and concentrated to give compound **21** (851 mg, 3.65 mmol) as a colorless oil in 80% yield, which was used in further steps without purification.

Compound 22 (56)

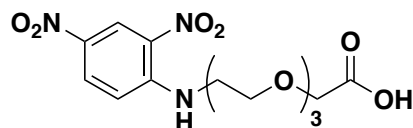
2-(2-(2-(2-aminoethoxy)ethoxy)ethoxy)acetic acid



Compound **21** (2.4 g, 10.3 mmol) was dissolved in methanol and the atmosphere flushed with N_2 . Palladium on carbon (240 mg, 10% w/w) was added, and the flask purged again with nitrogen. The flask was then purged with H_2 gas and stirred under H_2 atmosphere for 16 hours. The reaction then filtered through celite and concentrated to give compound **22** (2.13 g, 10.3 mmol) as a colorless oil in quantitative yield. Compound **22** was used in further steps without purification.

Compound 23

2-(2-(2-(2-((2,4-dinitrophenyl)amino)ethoxy)ethoxy)ethoxy)acetic acid



1-chloro-2,4-dinitrobenzene (52.8 mg, 0.261 mmol, 1.00 eq), compound **22** (75.5 mg, 0.365 mmol, 1.40 eq), and sodium bicarbonate (65.7 mg, 0.782 mmol, 3.00 eq) were dissolved in water (2 mL)

in a round bottom flask. The flask was then equipped with a reflux condenser and the mixture stirred at 95 °C for 16 hours. The reaction was then cooled and diluted into saturated sodium bicarbonate solution (10 mL), then washed with dichloromethane. The aqueous solution was then treated with concentrated hydrochloric acid until the pH of the solution was below 2. The aqueous layer was then extracted twice with dichloromethane. The combined organic layers were dried over sodium sulfate and concentrated to give compound **23** (86.8 mg, 0.232 mmol) as a bright yellow oil in 89% yield, which was used without further purification.

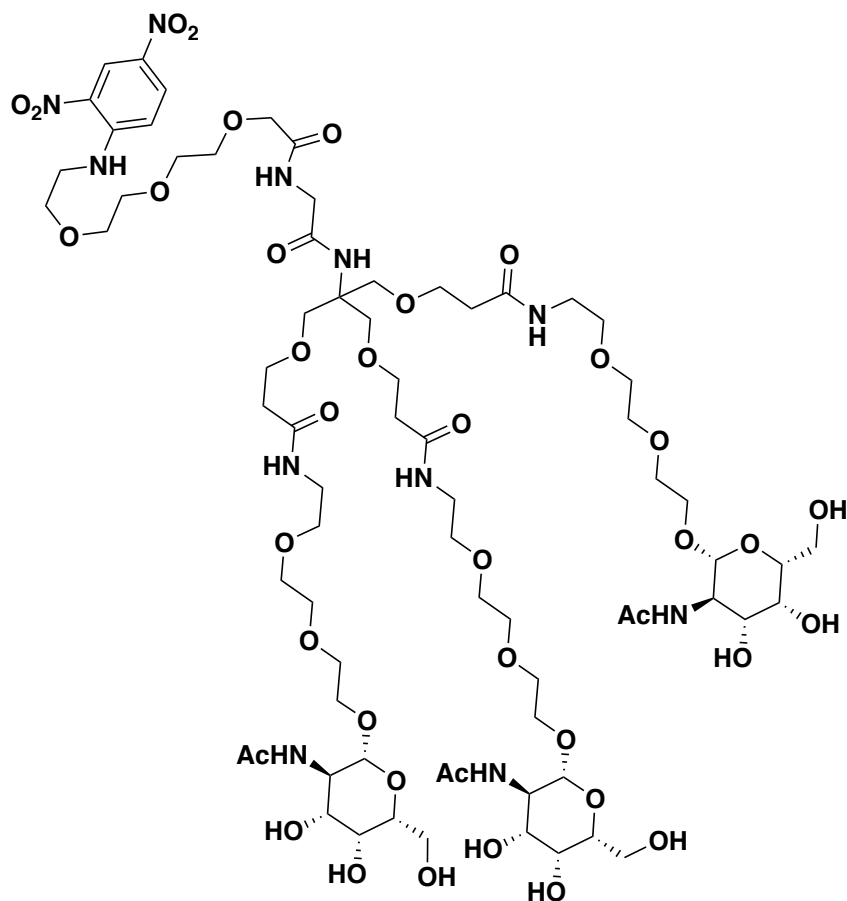
^1H NMR (400 MHz, DMSO- d_6) δ 12.59 (s, 1H), 8.86 (d, J = 2.8 Hz, 2H), 8.27 (dd, J = 9.6, 2.8 Hz, 1H), 7.29 (d, J = 9.7 Hz, 1H), 3.99 (s, 2H), 3.69 (dd, J = 6.3, 4.1 Hz, 4H), 3.62 – 3.50 (m, 8H).

^{13}C NMR (126 MHz, DMSO- d_6) δ 172.04, 148.83, 135.34, 130.33, 130.13, 124.02, 116.10, 70.24, 70.22, 70.18, 68.71, 68.05, 43.11.

HRMS: $[\text{M}+\text{H}]^+$ Expected 374.1200 Found 374.1198

IR, $f(\text{cm}^{-1})$: 3358, 2875, 1736, 1618, 1585, 1523, 1423, 1330, 1303, 1092, 744

Compound 24 (D-MoDE-A)



Compound **23** (75.1mg, 0.201 mmol, 1.5 eq) was dissolved in dichloromethane (7 mL) and diisopropylethylamine (26 mg, 0.201 mmol, 1.5 eq). 1-hydroxybenzotriazole hydrate (34.9 mg, 0.2278 mmol, 1.7 eq) and 1-Ethyl-3-(3-dimethylaminopropyl)carbodiimide (41.0 mg, 0.214 mmol, 1.6 eq) were then added and stirred for 10 minutes. Cbz-protected amine 9-OAc (238mg, 0.134 mmol, 1 eq) was added, then the reaction mixture stirred overnight. Mixture was diluted into dichloromethane (50 mL) and washed with water (2x) and brine (1x). The organic layer was dried over sodium sulfate and concentrated. The residue was dissolved in methanol (3.5 mL) and chilled to 0 °C. Sodium methoxide solution (5.4 M in methanol, 292 µL) was then added, and the reaction stirred at 0 °C for 30 minutes. It was then neutralized with Dowex 50WX8. The reaction was filtered and concentrated. The residue was directly purified on HPLC (0-30% acetonitrile in water, + 0.1% formic acid) to give compound **24** as a bright yellow powder in 18.6% yield (0.0249 mmol, 43.7 mg).

¹H NMR (500 MHz, DMSO-*d*₆) δ 8.86 (d, *J* = 2.7 Hz, 1H), 8.84 (d, *J* = 5.3 Hz, 1H), 8.26 (dd, *J* = 9.6, 2.8 Hz, 1H), 7.89 (t, *J* = 5.5 Hz, 3H), 7.71 (t, *J* = 5.8 Hz, 1H), 7.28 (d, *J* = 9.6 Hz, 1H), 7.22 (s, 1H), 4.52 – 4.46 (m, 2H), 3.90 (s, 2H), 3.75 – 3.63 (m, 8H), 3.63 – 3.45 (m, 36H), 3.44 – 3.36 (m, 10H), 3.20 (q, *J* = 5.8 Hz, 6H), 2.30 (t, *J* = 6.4 Hz, 6H).

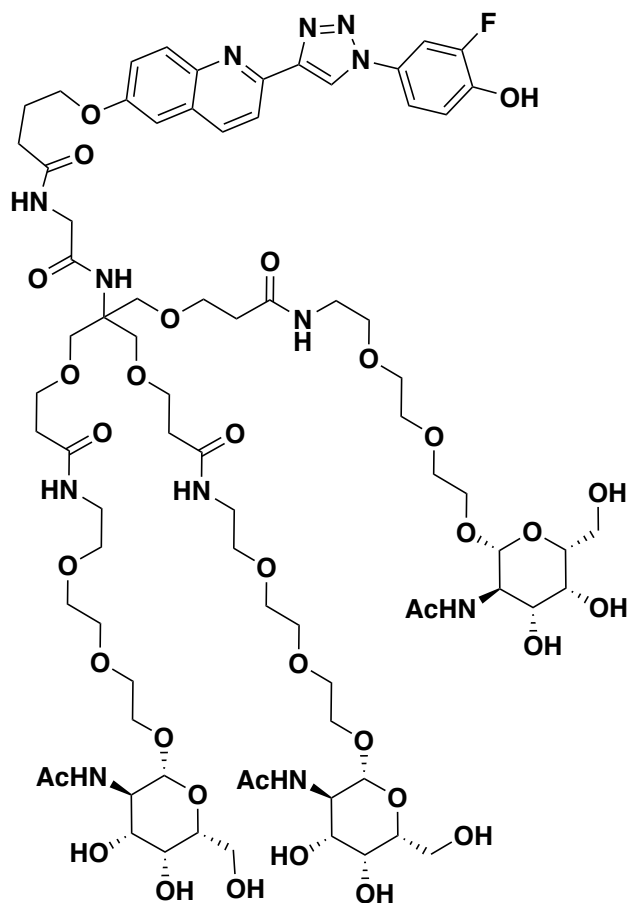
¹³C NMR (126 MHz, DMSO-*d*₆) δ 170.66, 169.75, 168.75, 148.81, 135.35, 130.32, 130.13, 123.99, 116.07, 72.77, 70.68, 70.30, 70.21, 70.12, 70.04, 69.92, 69.55, 68.70, 67.98, 67.87, 67.78, 60.66, 60.20, 43.11, 42.05, 38.96, 36.29.

HRMS: [M+H]⁺ Expected 1752.7901, Found 1752.7926

[α]_D = -15.46° (c = 1 g/100 mL, MeOH, 25.01 °C)

IR, *f*(cm⁻¹): 3300, 2874, 1641, 1620, 1550, 1429, 1370, 1336, 1308, 1070

Compound **25** (M-MoDE-A)



Compound **18** (23.5 mg, 0.0575 mmol, 1.1 eq) and (1-[Bis(dimethylamino)methylene]-1H-1,2,3-triazolo[4,5-b]pyridinium 3-oxide hexafluorophosphate (HATU) (20.0 mg, 0.0522 mmol, 1 eq) were dissolved in dry dimethylformamide (5 mL) and diisopropylethylamine (23.3 μ L, 16.9 mg, 0.131 mmol, 2.5 eq) and stirred for 10 minutes at room temperature. Compound **11** (73.0 mg, 0.0522 mmol) was then added, and the reaction stirred for 30 minutes. The mixture was loaded directly onto HPLC and purified (20-30% acetonitrile in water, +0.3% trifluoroacetic acid) to give compound **25** (12 mg, 0.0067 mmol) as an offwhite powder in 12.8% yield.

^1H NMR (600 MHz, $\text{DMSO-}d_6$) δ 9.33 (s, 1H), 8.42 (d, J = 8.6 Hz, 1H), 8.22 (d, J = 8.5 Hz, 1H), 8.10 (t, J = 5.9 Hz, 1H), 7.98 (d, J = 9.1 Hz, 1H), 7.94 (t, J = 5.7 Hz, 3H), 7.91 (dd, J = 11.7, 2.6 Hz, 1H), 7.70 (dd, J = 8.8, 2.5 Hz, 1H), 7.64 (d, J = 9.1 Hz, 3H), 7.48 – 7.42 (m, 2H), 7.18 (d, J = 9.0 Hz, 1H), 7.15 (d, J = 4.8 Hz, 1H), 4.28 (d, J = 8.4 Hz, 3H), 4.17 – 4.12 (m, 3H), 3.80 – 3.74 (m, 2H), 3.71 (t, J = 9.3 Hz, 6H), 3.65 (d, J = 3.0 Hz, 3H), 3.59 – 3.45 (m, 39H), 3.43 (dd, J = 10.6, 3.1 Hz, 3H), 3.39 (t, J = 6.0 Hz, 6H), 3.31 (t, J = 6.2 Hz, 3H), 3.20 (q, J = 5.9 Hz, 6H), 2.37 (t, J = 7.4 Hz, 2H), 2.31 (t, J = 6.4 Hz, 6H), 2.04 (p, J = 6.9 Hz, 2H), 1.80 (s, 9H).

^{13}C NMR (151 MHz, $\text{DMSO-}d_6$) δ 172.43, 170.74, 170.00, 169.29, 157.04, 152.11, 150.50, 148.61, 147.82, 143.81, 136.44, 130.37, 129.01, 123.25, 121.75, 119.04, 118.72, 117.28, 109.76, 109.60, 107.09, 101.79, 75.73, 71.99, 70.14, 70.04, 69.99, 69.53, 68.69, 68.00, 67.90, 67.82, 67.76, 60.87, 60.10, 52.37, 42.61, 38.95, 36.27, 31.93, 25.18, 23.48.

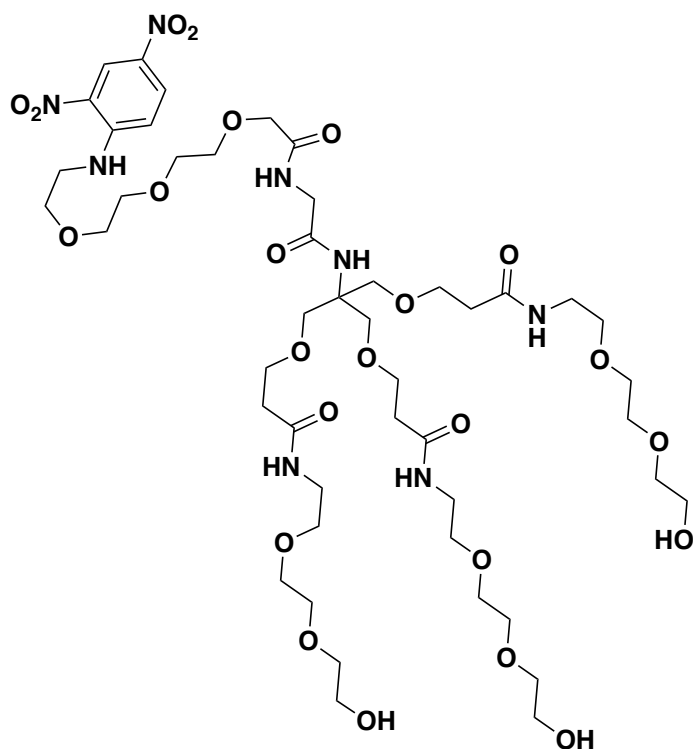
HRMS: $[M+H]^+$ Expected 1787.804, Found 1787.799

$[\alpha]_D = -15.90^\circ$ ($c = 1$ g/100 mL, MeOH, 23.52 °C)

IR $f(\text{cm}^{-1})$: 3291, 3089, 2881, 1641, 1548, 1531, 1427, 1373, 1301, 1250, 1201, 1035

Compound 26 (DNP-OH3)

3,3'-((2-(14-((2,4-dinitrophenyl)amino)-4-oxo-6,9,12-trioxa-3-azatetradecanamido)-2-(14-hydroxy-5-oxo-2,9,12-trioxa-6-azatetradecyl)propane-1,3-diyl)bis(oxy))bis(*N*-(2-(2-(2-hydroxyethoxy)ethoxy)ethyl)propanamide)



Compound **13** (234 mg, 0.297 mmol, 1 eq) was dissolved in dimethylformamide (5 mL) and triethylamine (83 μL , 0.594 mmol, 2 eq). Compound **23** (110.9 mg, 0.297 mmol, 1 eq) and 1-Hydroxybenzotriazole hydrate (59 mg, 0.386 mmol, 1.3 eq) were then added, followed by 1-ethyl-3-(3-dimethylaminopropyl)carbodiimide (68.3 mg, 0.356 mmol, 1.2 eq). The reaction was stirred overnight, then evaporated under a stream of nitrogen. Product was purified directly via reverse phase HPLC (0-30% acetonitrile in water +0.1% formic acid) to give compound **26** (178 mg, 0.155 mmol) as a bright yellow powder in 52.3% yield.

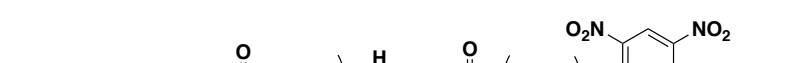
^1H NMR (500 MHz, $\text{DMSO}-d_6$) δ 8.86 (d, $J = 2.7$ Hz, 1H), 8.84 (d, $J = 5.3$ Hz, 1H), 8.26 (dd, $J = 9.6, 2.8$ Hz, 1H), 7.89 (t, $J = 5.5$ Hz, 3H), 7.71 (t, $J = 5.8$ Hz, 1H), 7.28 (d, $J = 9.6$ Hz, 1H), 7.22 (s, 1H), 4.52 – 4.46 (m, 2H), 3.90 (s, 2H), 3.75 – 3.63 (m, 8H), 3.63 – 3.45 (m, 36H), 3.44 – 3.36 (m, 10H), 3.20 (q, $J = 5.8$ Hz, 6H), 2.30 (t, $J = 6.4$ Hz, 6H).

^{13}C NMR (126 MHz, $\text{DMSO-}d_6$) δ 170.66, 169.75, 168.75, 148.81, 135.35, 130.32, 130.13, 123.99, 116.07, 72.77, 70.68, 70.30, 70.21, 70.12, 70.04, 69.92, 69.55, 68.70, 67.98, 67.87, 67.78, 60.66, 60.20, 43.11, 42.05, 38.96, 36.29.

HRMS: $[\text{M}+\text{Na}]^+$ Expected 1165.5340, Found 1165.5339

IR $f(\text{cm}^{-1})$: 3340, 2875, 1650, 1620, 1585, 1545, 1525, 1425, 1336, 1304, 1201, 1091, 923

A



DNP-OH3

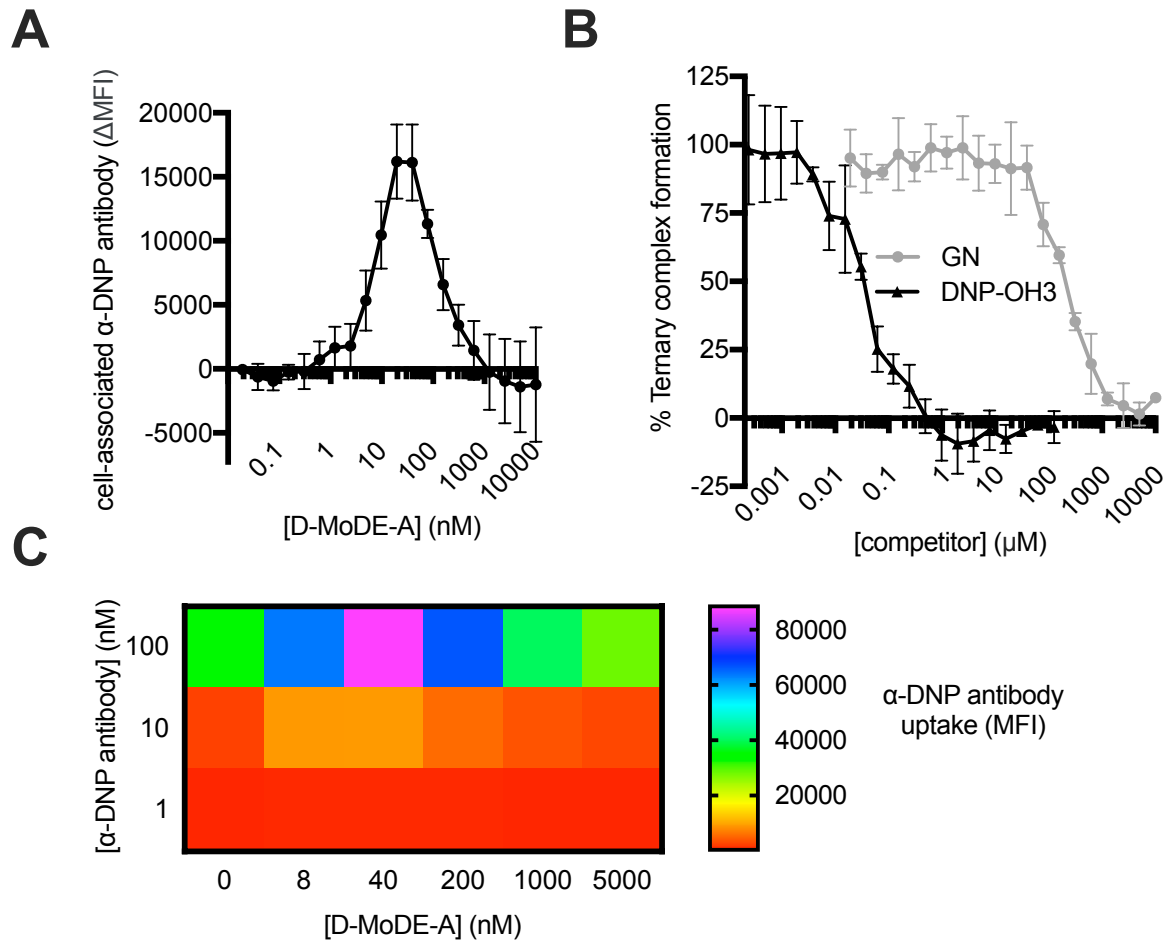
A) Chemical structure of α -DNP antibody binding control molecule DNP-OH3

[illegible]

DNP-OH3

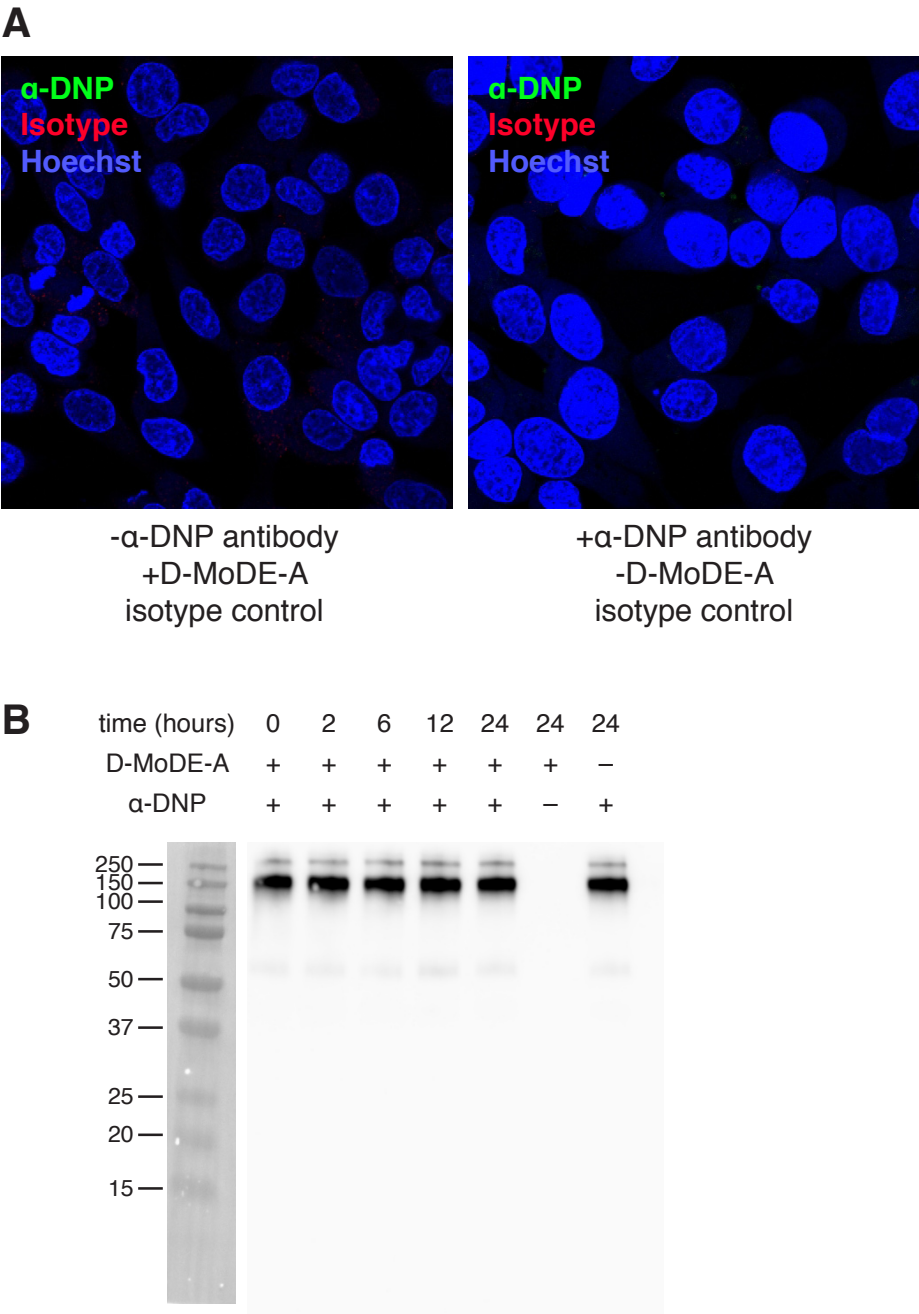
A) Chemical structure of α -DNP antibody binding control molecule DNP-OH3

Fig. S2.



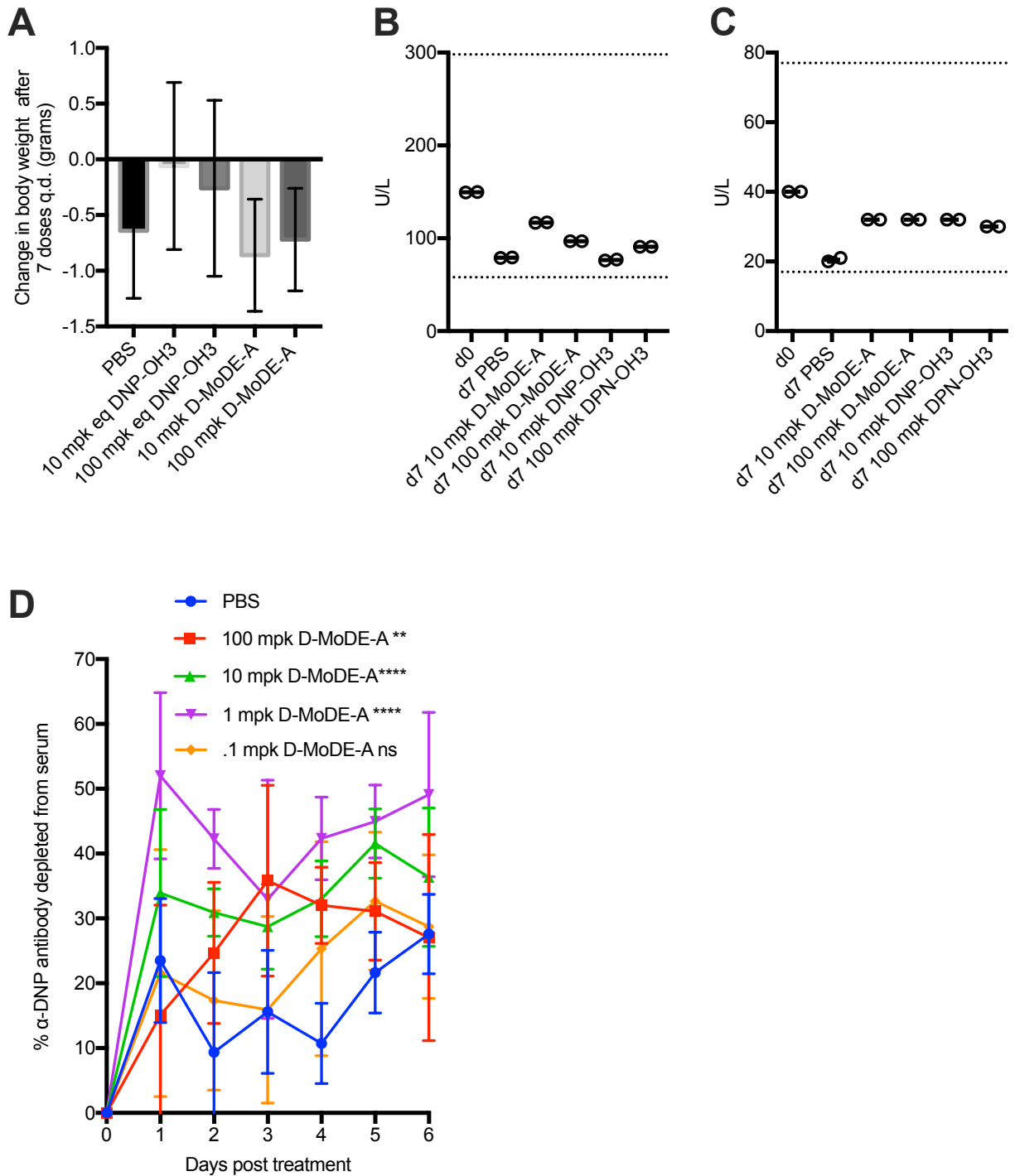
- A) Formation of a ternary complex between hepatocytes and α -DNP antibody is dependent on the concentration of D-MoDE-A.
- B) D-MoDE-A-mediated ternary complex formation is inhibited by competitive binders of either ASGPR or α -DNP antibody.
- C) Endocytosis of α -DNP antibody in hepatocytes is dependent on both α -DNP antibody and D-MoDE-A concentration (12 hour time point).

Fig. S3.



A) Alexa 488 signal in colocalization studies is dependent on the presence of α -DNP antibody and D-MoDE-A. Primary antibody is necessary for EEA1/LAMP2 signal.
B) Representative western blot of cell culture supernatants.

Fig. S4.



A) Mouse body weight following treatment with D-MoDE-A or DNP-OH3 (data from study in figure 4B). Statistical differences were analyzed by T test.

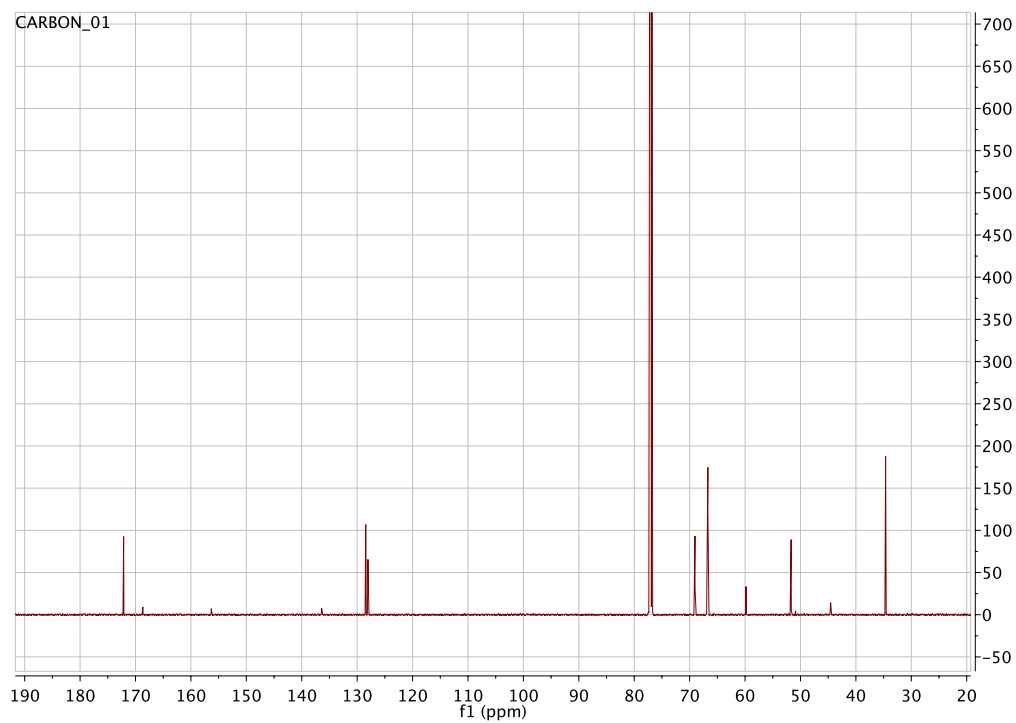
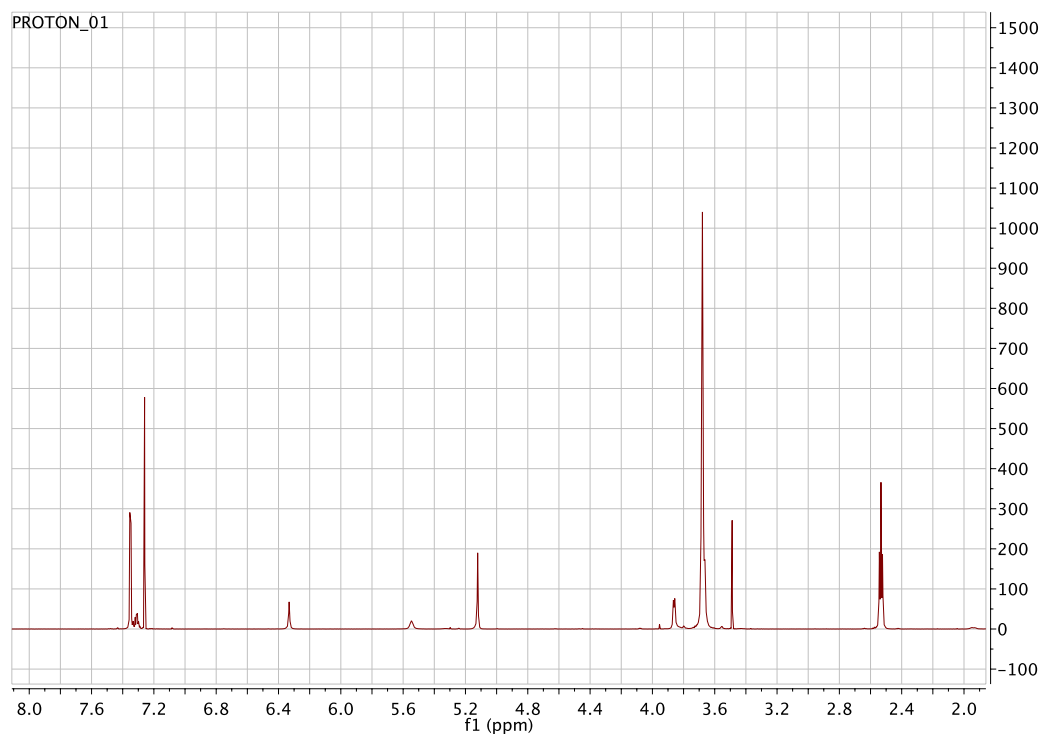
B) Levels of aspartate transaminase (AST) in treated mice (data from pooled serum from study in figure 4B). Dashed lines represent the normal range.

C) Levels of alanine transaminase (ALT) in treated mice (data from pooled serum from study in figure 4B). Dashed lines represent the normal range.

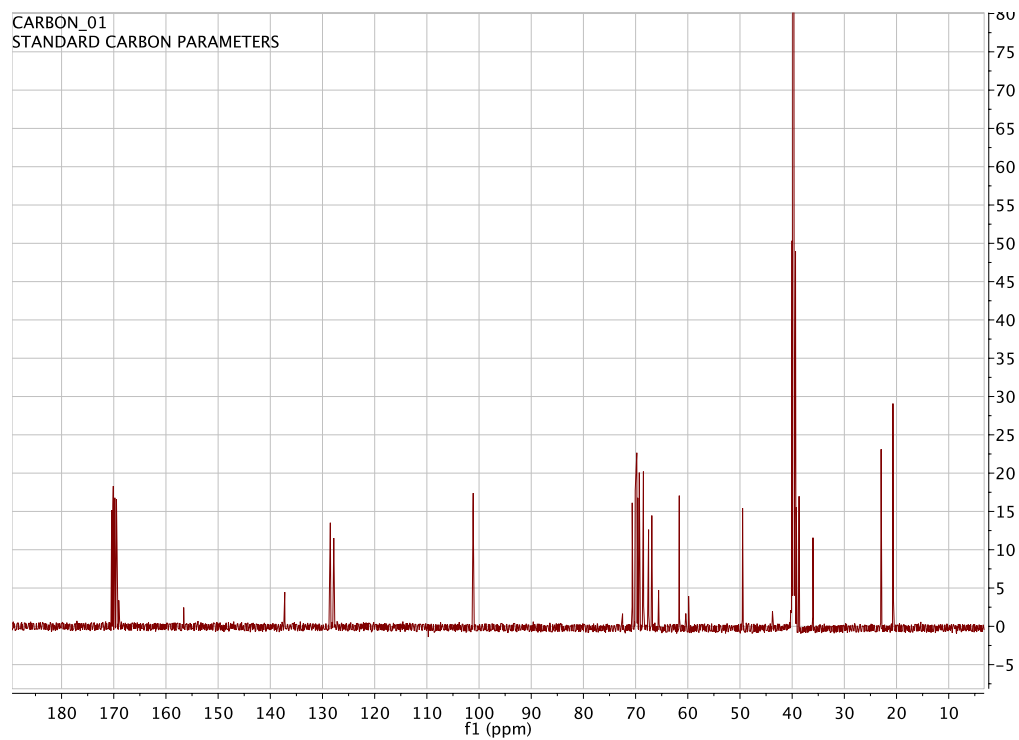
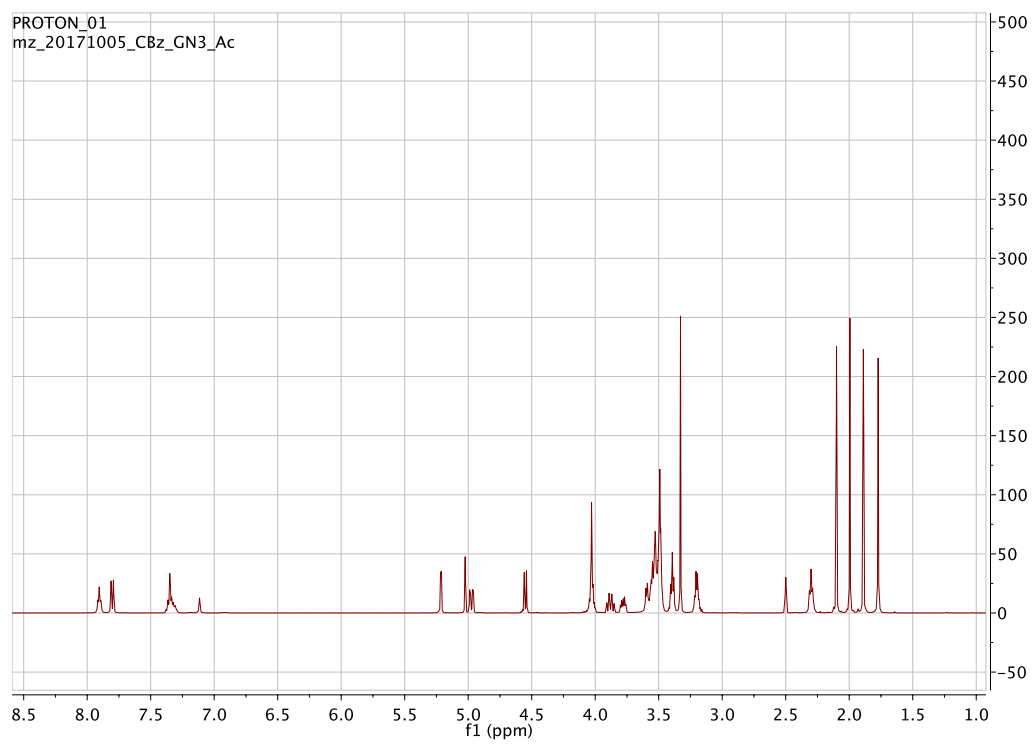
D) Decrease in serum levels of α -DNP antibody following a single variable dose of D-MoDE-A. Each experimental group contained at least eight mice. Statistical differences were assessed by repeated measures two-way ANOVA with Tukey's tests for post-hoc comparison of simple effects between each of the treatment groups and PBS.

Spectral data

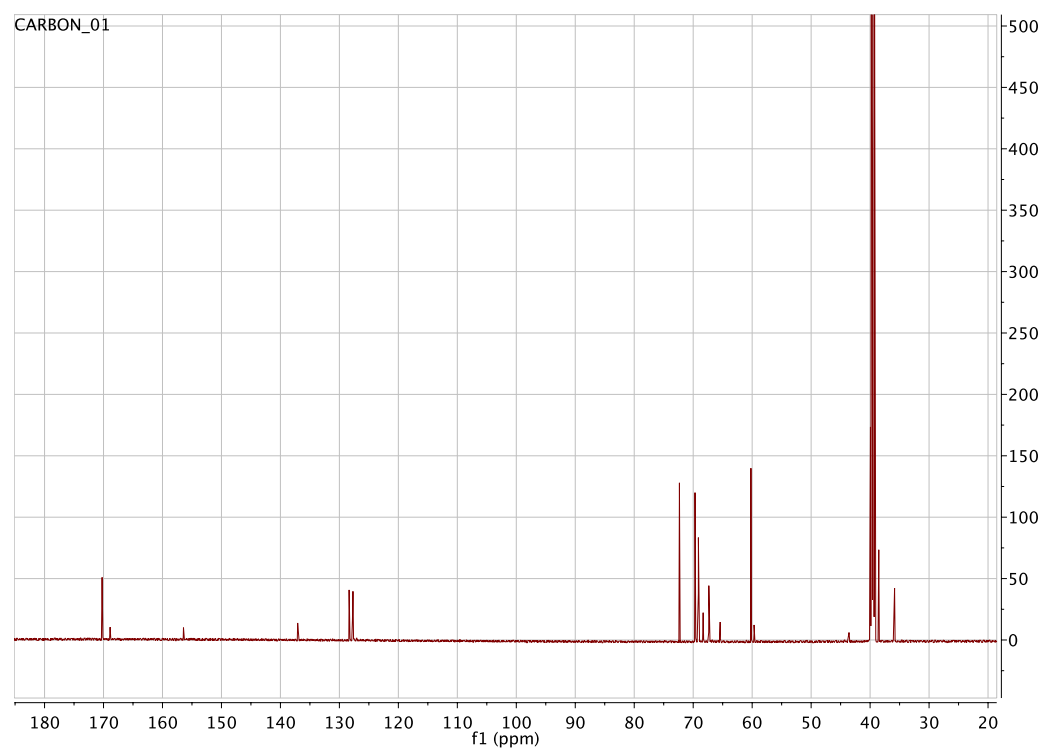
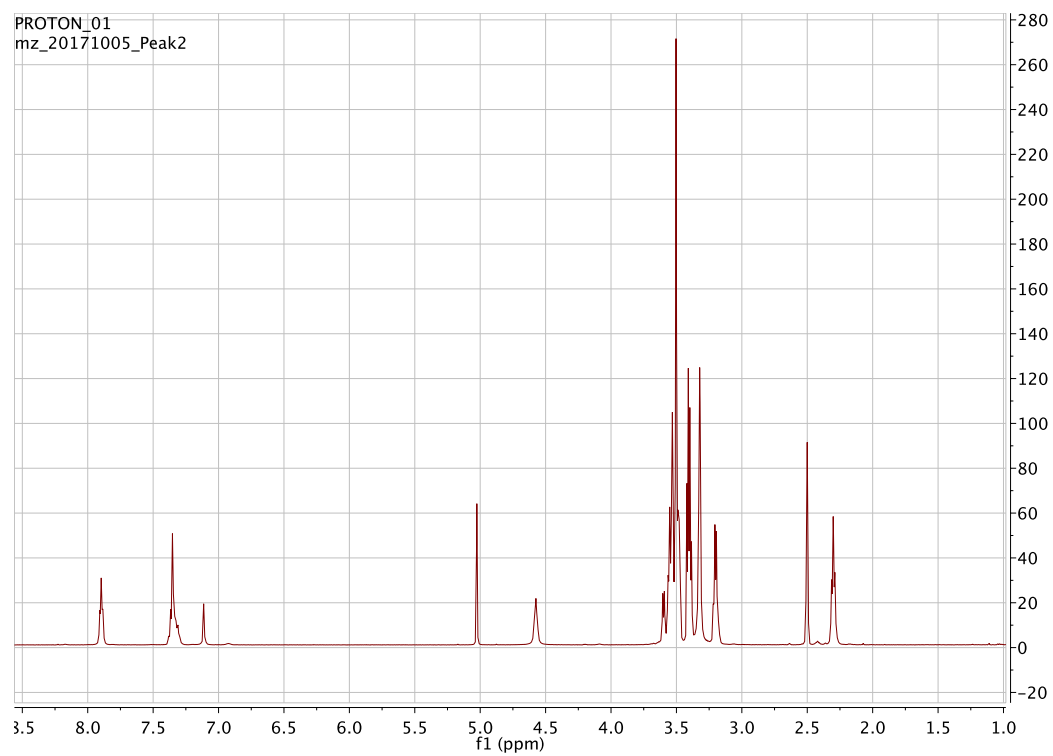
Compound 8



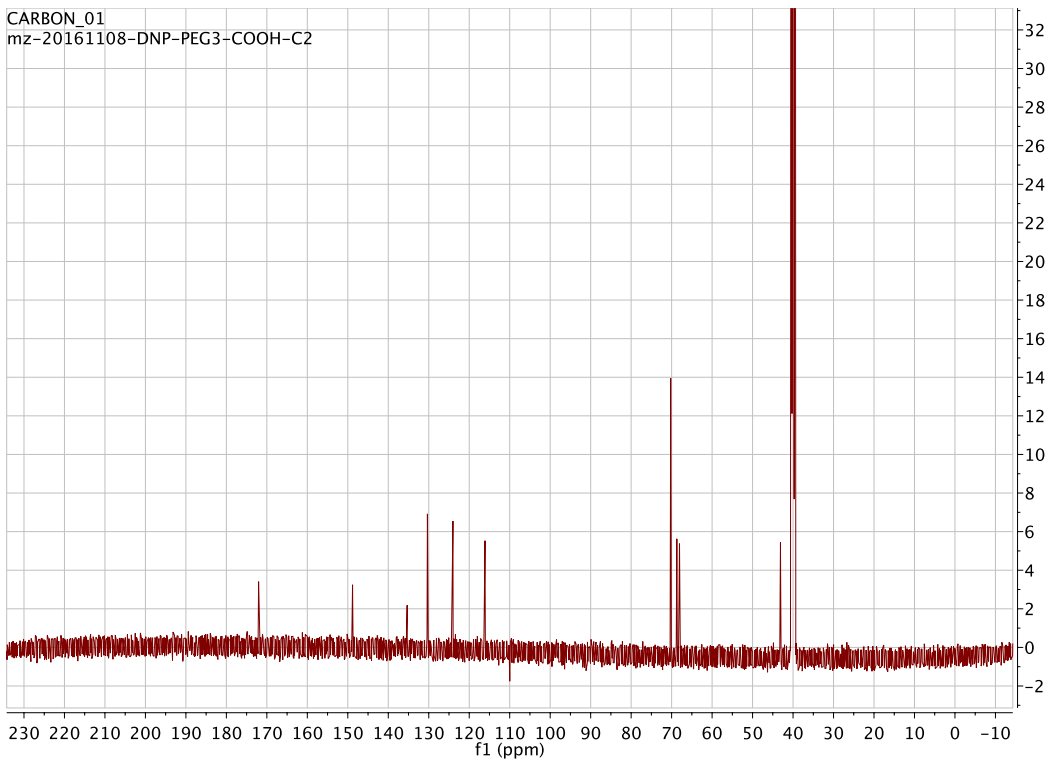
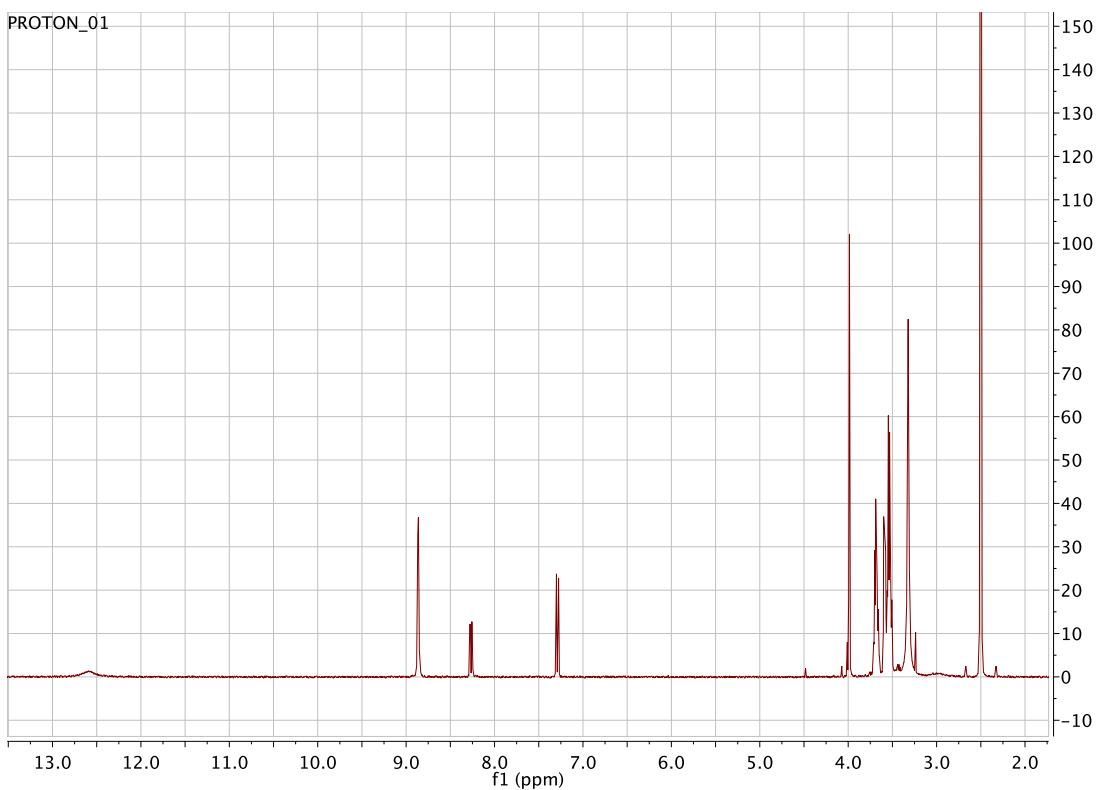
Compound 10



Compound 12

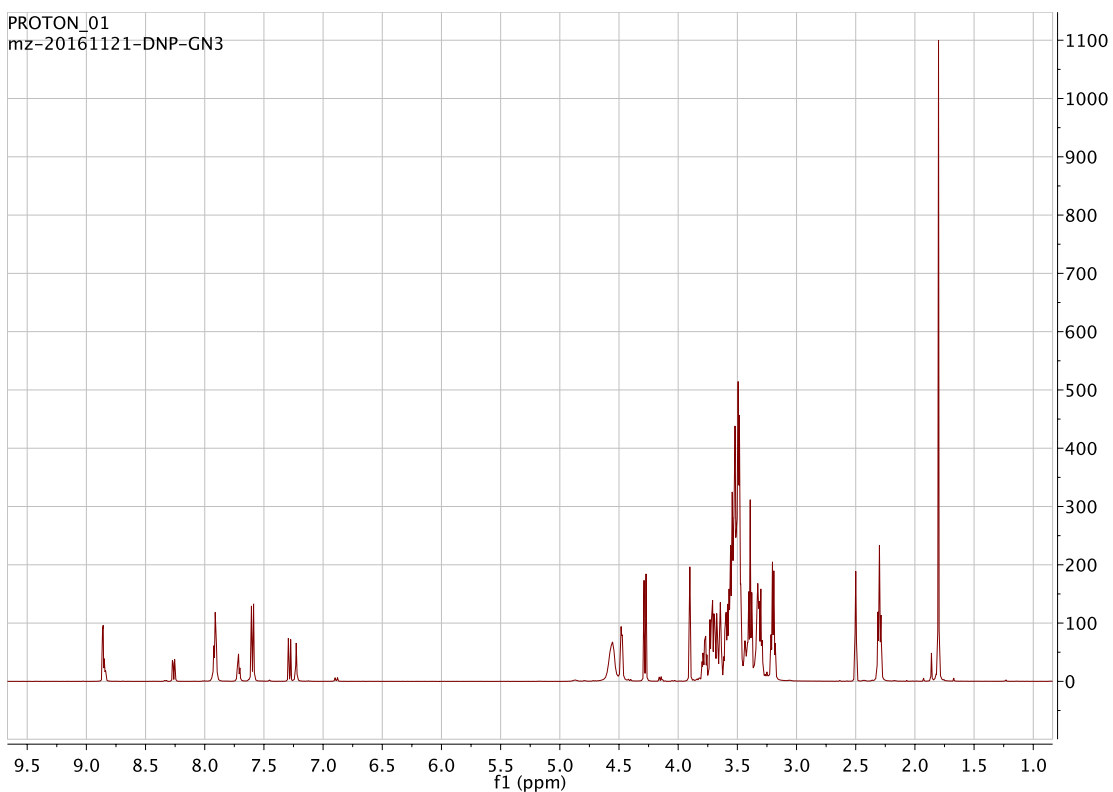


Compound 23

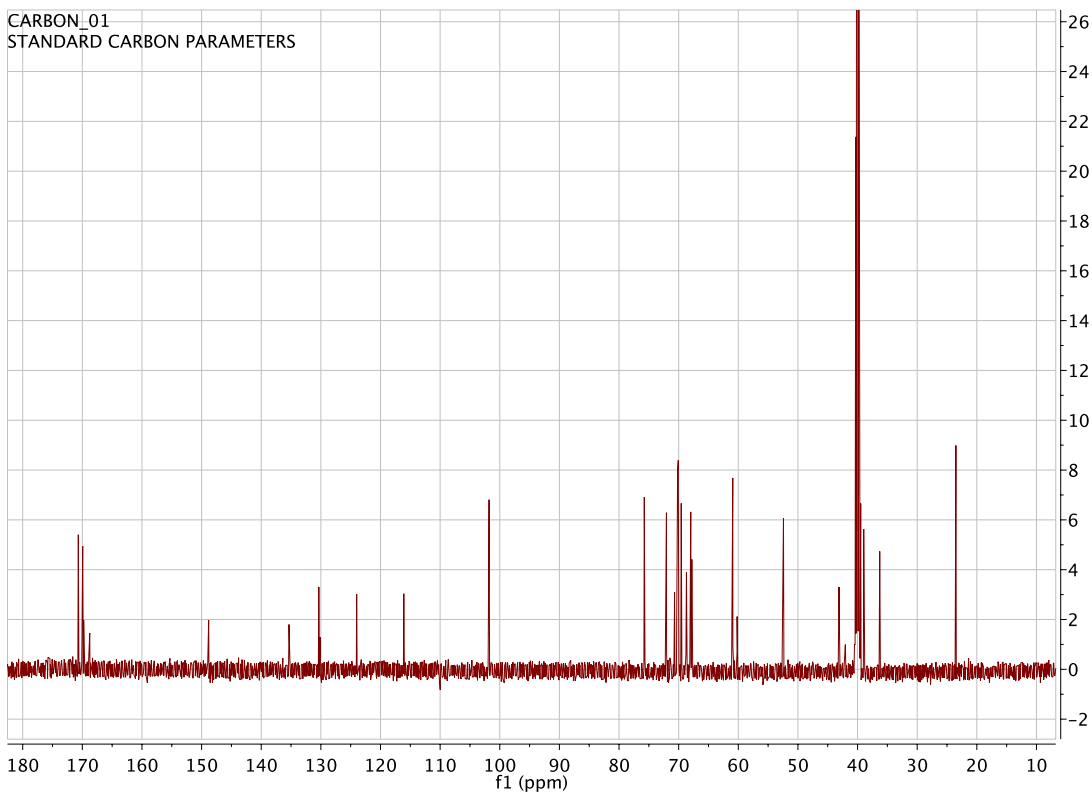


Compound 24

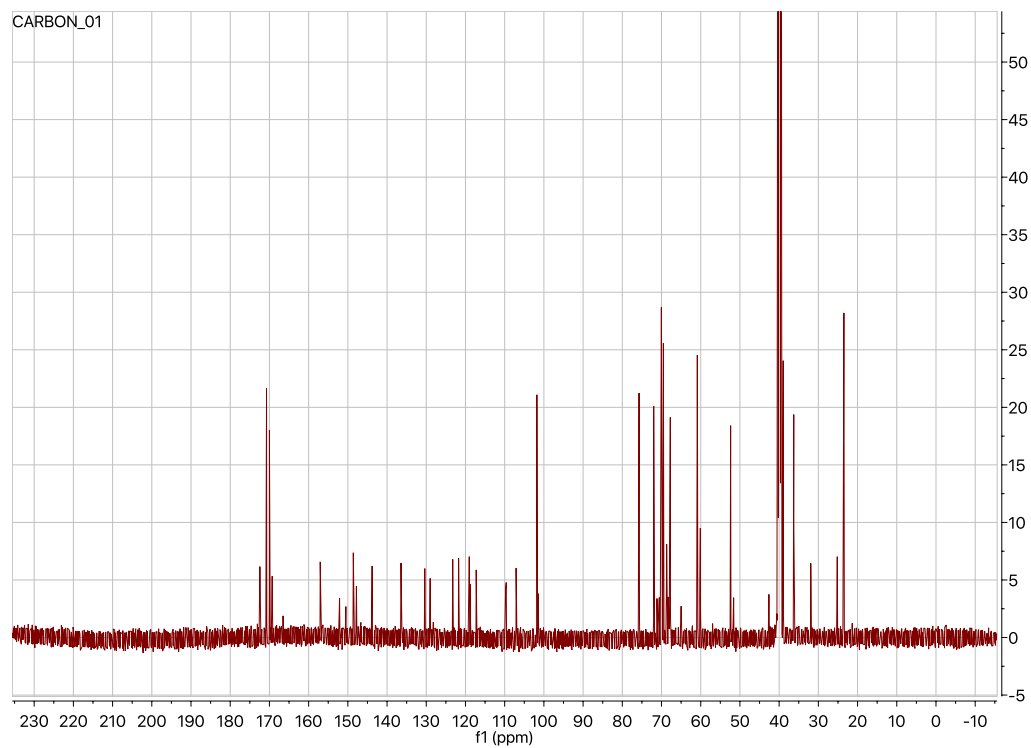
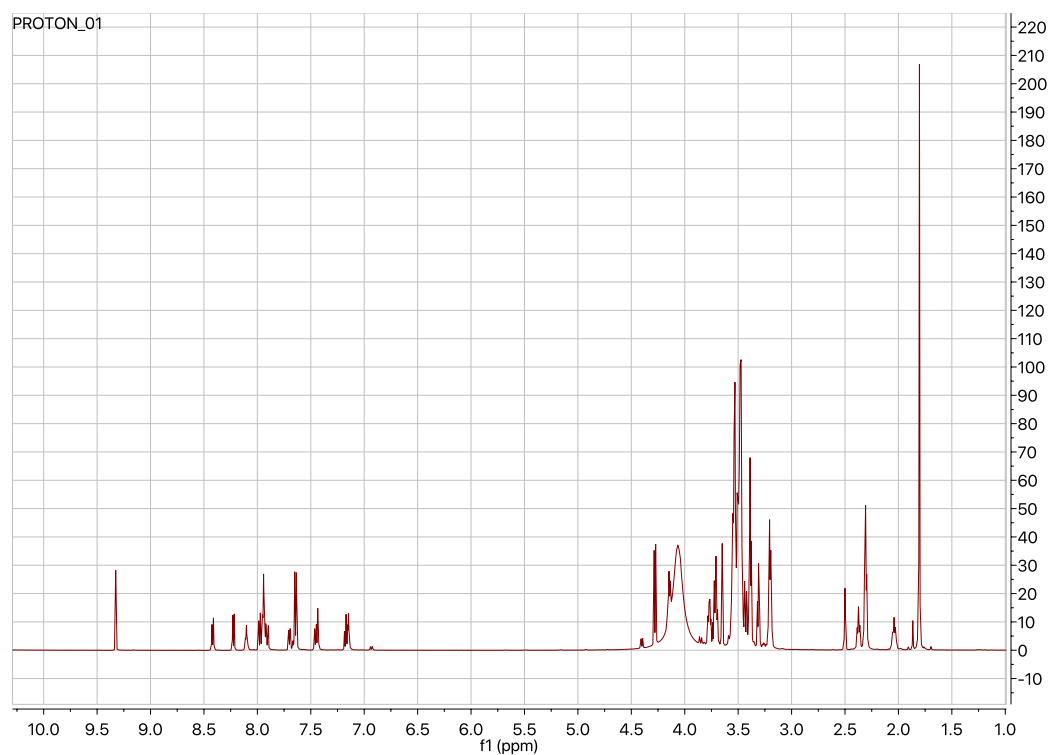
PROTON_01
mz-20161121-DNP-GN3



CARBON_01
STANDARD CARBON PARAMETERS

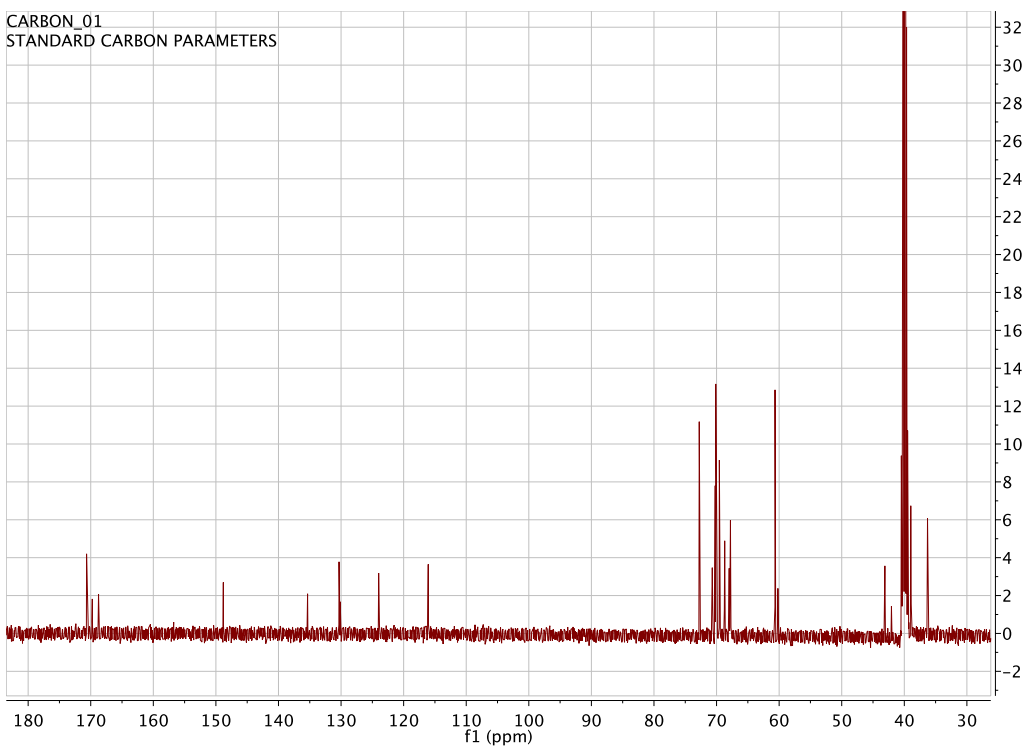


Compound 25

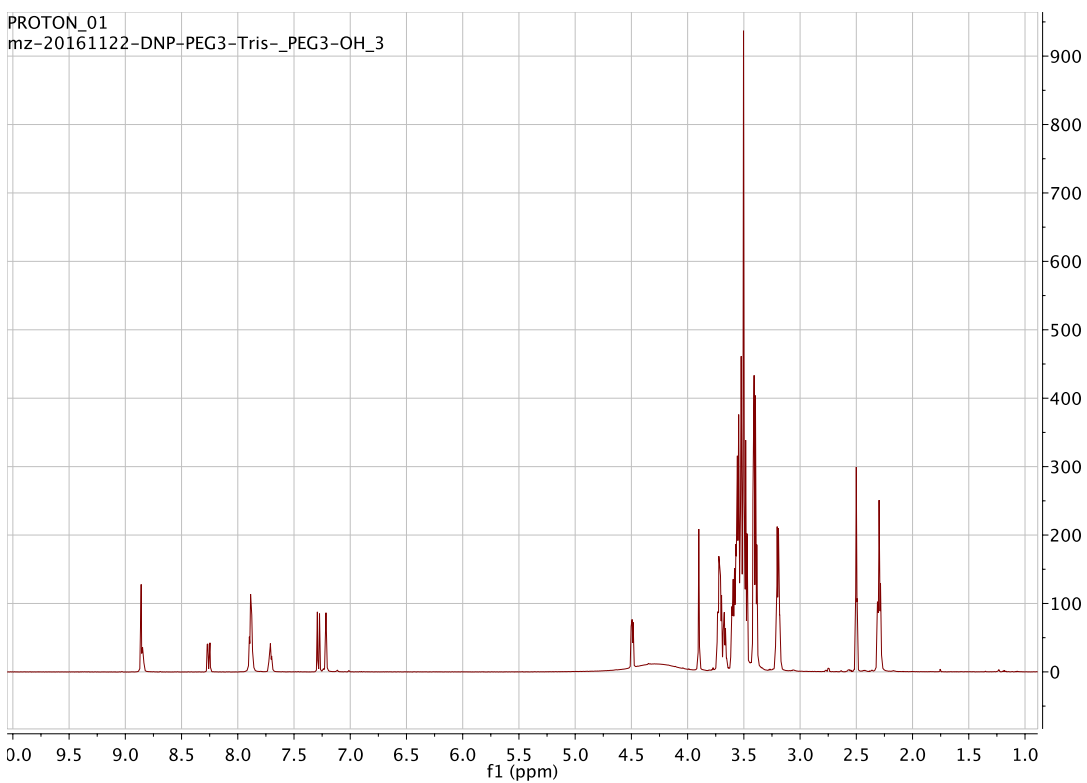


Compound 26

CARBON_01
STANDARD CARBON PARAMETERS



PROTON_01
mz-20161122-DNP-PEG3-Tris-_PEG3-OH_3



Full reference list

1. B. Chen, X. Shi, Y. Cui, A. Hou, P. Zhao, A Review of PCSK9 Inhibitors and their Effects on Cardiovascular Diseases. *Curr. Top. Med. Chem.* **19**, 1790-1817 (2019).
2. G. D. Kalliolias, L. B. Ivashkiv, TNF biology, pathogenic mechanisms and emerging therapeutic strategies. *Nat. Rev. Rheumatol.* **12**, 49 (2016).
3. J. B. Bilsborrow, E. Doherty, P. V. Tilstam, R. Bucala, Macrophage migration inhibitory factor (MIF) as a therapeutic target for rheumatoid arthritis and systemic lupus erythematosus. *Expert Opin. Ther.* **23**, 733-744 (2019).
4. J. Martínez-Fábregas, A. Prescott, S. van Kasteren, D. L. Pedrioli, I. McLean, A. Moles, T. Reinheckel, V. Poli, C. Watts, Lysosomal protease deficiency or substrate overload induces an oxidative-stress mediated STAT3-dependent pathway of lysosomal homeostasis. *Nat. Commun.* **9**, 5343 (2018).
5. C. Zoja, A. Benigni, G. Remuzzi, Protein overload activates proximal tubular cells to release vasoactive and inflammatory mediators. *Nephron Exp. Nephrol.* **7**, 420-428 (1999).
6. H. Nakajima, M. Takenaka, J. Y. Kaimori, T. Hamano, H. Iwatani, T. Sugaya, T. Ito, M. Hori, E. Imai, Activation of the signal transducer and activator of transcription signaling pathway in renal proximal tubular cells by albumin. *J. Am. Soc. Nephrol.* **15**, 276-285 (2004).
7. M. Tanowitz, L. Hettrick, A. Revenko, G. A. Kinberger, T. P. Prakash, P. P. Seth, Asialoglycoprotein receptor 1 mediates productive uptake of N-acetylgalactosamine-conjugated and unconjugated phosphorothioate antisense oligonucleotides into liver hepatocytes. *Nucleic Acids Res.* **45**, 12388-12400 (2017).
8. P. K. Grewal, "The Ashwell-Morell Receptor" in *Methods in Enzymology*. (Elsevier, 2010), vol. 479, pp. 223-241.
9. Y. Mi, A. Lin, D. Fiete, L. Steirer, J. U. Baenziger, Modulation of mannose and asialoglycoprotein receptor expression determines glycoprotein hormone half-life at critical points in the reproductive cycle. *J. Biol. Chem.* **289**, 12157-12167 (2014).
10. W. H. Yang, P. V. Aziz, D. M. Heithoff, M. J. Mahan, J. W. Smith, J. D. Marth, An intrinsic mechanism of secreted protein aging and turnover. *Proc. Natl. Acad. Sci.* **112**, 13657-13662 (2015).
11. L. M. Steirer, E. I. Park, R. R. Townsend, J. U. Baenziger, The asialoglycoprotein receptor regulates levels of plasma glycoproteins terminating with sialic acid α 2, 6-galactose. *J. Biol. Chem.* **284**, 3777-3783 (2009).
12. R. Grozovsky, A. J. Begonja, K. Liu, G. Visner, J. H. Hartwig, H. Falet, K. M. Hoffmeister, The Ashwell-Morell receptor regulates hepatic thrombopoietin production via JAK2-STAT3 signaling. *Nat. Med.* **21**, 47 (2015).
13. X. Huang, J. C. Leroux, B. Castagner, Well-defined multivalent ligands for hepatocytes targeting via asialoglycoprotein receptor. *Bioconjugate Chem.* **28**, 283-295 (2016).
14. A. A. D'Souza, P. V. Devarajan, Asialoglycoprotein receptor mediated hepatocyte targeting—strategies and applications. *J. Control. Release* **203**, 126-139 (2015).
15. S. Matsuda, K. Keiser, J. K. Nair, K. Charisse, R. M. Manoharan, P. Kretschmer, C. G. Peng, A. V. Kel'in, P. Kandasamy, J. L. S. Willoughby, A. Liebow, W. Querbes, K. Yucius, T. Nguyen, S. Milstein, M. A. Maier, K. G. Rajeev, M. Manoharan, siRNA conjugates carrying sequentially assembled trivalent N-acetylgalactosamine linked

- through nucleosides elicit robust gene silencing in vivo in hepatocytes. *ACS Chem. Biol.* **10**, 1181-1187 (2015).
16. E. A. Biessen, A. R. Valentijn, R. L. De Vruhe, E. Van De Bilt, L. A. Sliedregt, P. Prince, M. K. Bijsterbosch, J. H. Van Boom, G. A. Van Der Marel, P. J. Abrahams, T. J. Van Berkel, Novel hepatotrophic prodrugs of the antiviral nucleoside 9-(2-phosphonylmethoxyethyl) adenine with improved pharmacokinetics and antiviral activity. *FASEB J.* **14**, 1784-1792 (2000).
 17. A. M. Pujol, M. Cuillel, O. Renaudet, C. Lebrun, P. Charbonnier, D. Cassio, C. Gateau, P. Dumy, E. Mintz, P. Delangle, Hepatocyte targeting and intracellular copper chelation by a thiol-containing glycocyclopeptide. *J. Am. Chem. Soc.* **133**, 286-296 (2010).
 18. A. Akinc, W. Querbes, S. De, J. Qin, M. Frank-Kamenetsky, K. N. Jayaprakash, M. Jayaraman, K. G. Rajeev, W. L. Cantley, J. R. Dorkin, J. S. Butler, L. Qin, T. Racie, A. Sprague, E. Fava, A. Zeigerer, M. J. Hope, M. Zerial, D. W. Y. Sah, K. Fitzgerald, M. A. Tracy, M. Manoharan, V. Kotliansky, A. de Fuogerolles, M. A. Maier, Targeted delivery of RNAi therapeutics with endogenous and exogenous ligand-based mechanisms. *Mol. Ther.* **18**, 1357-1364 (2010).
 19. V. Bocci, The role of sialic acid in determining the life-span of circulating cells and glycoproteins. *Experientia* **32**, 135-140 (1976).
 20. J. U. Baenziger, D. Fiete, Galactose and N-acetylgalactosamine-specific endocytosis of glycopeptides by isolated rat hepatocytes. *Cell* **22**, 611-620 (1980).
 21. J. R. Merwin, G. S. Noell, W. L. Thomas, H. C. Chiou, M. E. DeRome, T. D. McKee, G. L. Spitalny, M. A. Findeis, Targeted delivery of DNA using YEE (GalNAcAH)₃, a synthetic glycopeptide ligand for the asialoglycoprotein receptor. *Bioconjugate Chem.* **5**, 612-620 (1994).
 22. P.C. Rensen, L. A. Sliedregt, M. Ferns, E. Kieviet, S. M. Van Rossenberg, S. H. van Leeuwen, T. J. Van Berkel, E. A. Biessen, Determination of the upper size limit for uptake and processing of ligands by the asialoglycoprotein receptor on hepatocytes *in vitro* and *in vivo*. *J. Biol. Chem.* **276**, 37577-37584 (2001).
 23. S. K. Mamidyalala, S. Dutta, B. A. Chrnyk, C. Prévile, H. Wang, J. M. Withka, A. McColl, T. A. Subashi, S. J. Hawrylik, M. C. Griffor, S. Kim, J. A. Pfefferkorn, D. A. Price, E. Menhaji-Klotz, V. Mascitti, M. G. Finn, Glycomimetic ligands for the human asialoglycoprotein receptor. *J. Am. Chem. Soc.* **134**, 1978-1981 (2012).
 24. T. Onizuka, H. Shimizu, Y. Moriwaki, T. Nakano, S. Kanai, I. Shimada, H. Takahashi, NMR study of ligand release from asialoglycoprotein receptor under solution conditions in early endosomes. *FEBS J.* **279**, 2645-2656 (2012).
 25. J. H. LaBadie, K. P. Chapman, N. N. Aronson, Glycoprotein catabolism in rat liver: Lysosomal digestion of iodinated asialo-fetuin. *Biochem. J.* **152**, 271-279 (1975).
 26. J. A. Cisneros, M. J. Robertson, M. Valhondo, W. L. Jorgensen, A fluorescence polarization assay for binding to macrophage migration inhibitory factor and crystal structures for complexes of two potent inhibitors. *J. Am. Chem. Soc.* **138**, 8630-8638 (2016).
 27. E. F. Douglass Jr, C. J. Miller, G. Sparer, H. Shapiro, D. A. Spiegel, A comprehensive mathematical model for three-body binding equilibria. *J. Am. Chem. Soc.* **135**, 6092-6099 (2013).
 28. W. Brown, N. Saunders, K. Møslgård, K. Dziegielewska, Fetuin—an old friend revisited. *BioEssays* **14**, 749-755 (1992).

29. C. L. Fernandes, R. Ligabue-Braun, H. Verli, Structural glycobiology of human α_1 -acid glycoprotein and its implications for pharmacokinetics and inflammation. *Glycobiology* **25**, 1125-1133 (2015).
30. B. Shi, M. Abrams, L. Sepp-Lorenzino, Expression of Asialoglycoprotein Receptor 1 in Human Hepatocellular Carcinoma. *J Histochem. Cytochem.* **61**, 901-909 (2013).
31. A. Cooper, Y. Shaul, Clathrin-mediated endocytosis and lysosomal cleavage of hepatitis B virus capsid-like core particles. *J. Biol. Chem.* **281**, 16563-16569 (2006).
32. S. Guo, X. Zhang, M. Zheng, X. Zhang, C. Min, Z. Wang, S. H. Cheon, M. H. Oak, S. Y. Nah, K. M. Kim, Selectivity of commonly used inhibitors of clathrin-mediated and caveolae-dependent endocytosis of G protein-coupled receptors. *BBA-Biomembranes* **1848**, 2101-2110 (2015).
33. L. D. Cervia, C. C. Chang, L. Wang, F. Yuan, Distinct effects of endosomal escape and inhibition of endosomal trafficking on gene delivery via electrotransfection. *PloS One* **12** (2017).
34. R. Ippoliti, P. Ginobbi, E. Lendaro, I. D'Agostino, D. Ombres, P. A. Benedetti, M. Brunori, G. Citro, The effect of monensin and chloroquine on the endocytosis and toxicity of chimeric toxins. *Cell. Mol. Life Sci.* **54**, 866-875 (1998).
35. Q. Ba, N. Zhou, J. Duan, T. Chen, M. Hao, X. Yang, J. Li, J. Yin, R. Chu, H. Wang, Dihydroartemisinin exerts its anticancer activity through depleting cellular iron via transferrin receptor-1. *PloS One* **7** (2012).
36. M. M. Zegers, K. J. Zaal, S. C. van IJzendoorn, K. Klappe, D. Hoekstra, Actin filaments and microtubules are involved in different membrane traffic pathways that transport sphingolipids to the apical surface of polarized HepG2 cells. *Mol. Biol. Cell* **9**, 1939-1949 (1998).
37. R. Maidorn, E. Cragoe, I. Tannock, Therapeutic potential of analogues of amiloride: inhibition of the regulation of intracellular pH as a possible mechanism of tumour selective therapy. *Br. J. Cancer* **67**, 297-303 (1993).
38. J. Oka, M. Christensen, P. Weigel, Hyperosmolarity inhibits galactosyl receptor-mediated but not fluid phase endocytosis in isolated rat hepatocytes. *J. Biol. Chem.* **264**, 12016-12024 (1989).
39. A. L. Schwartz, A. Bolognesi, S. E. Fridovich, Recycling of the asialoglycoprotein receptor and the effect of lysosomotropic amines in hepatoma cells. *J. Cell Biol.* **98**, 732-738 (1984).
40. K. Bridges, J. Harford, G. Ashwell, R. D. Klausner, Fate of receptor and ligand during endocytosis of asialoglycoproteins by isolated hepatocytes. *Proc. Natl. Acad. Sci.* **79**, 350-354 (1982).
41. S. Jevsevar, M. Kunstelj, "Half-life extension through PEGylation" in *Therapeutic Proteins: Strategies to Modulate Their Plasma Half-lives*, R. Kontermann, Ed. (Wiley-Blackwell, 2012), chap. 3.
42. S. Banik, K. Pedram, S. Wisnovsky, N. Riley, C. Bertozzi, https://chemrxiv.org/articles/preprint/Lysosome_Targeting_Chimeras_LYTACs_for_the_Degradation_of_Secreted_and_Membrane_Proteins/7927061/2 (2019).
43. X. Sun, H. Gao, Y. Yang, M. He, Y. Wu, Y. Song, Y. Tong, Y. Rao, PROTACs: great opportunities for academia and industry. *Sig. Transduct. Target Ther.* **4**, 64 (2019).
44. C. S. Guy, S. L. Rankin, T. I. Michalak, Hepatocyte cytotoxicity is facilitated by asialoglycoprotein receptor. *Hepatol.* **54**, 1043-1050 (2011).

45. V. Benseler, A. Warren, M. Vo, L. E. Holz, S. S. Tay, D. G. Le Couteur, E. Breen, A. C. Allison, N. van Rooijen, C. McGuffog, H. J. Schlitt, D. G. Bowen, G. W. McCaughan, P. Bertolino, Hepatocyte entry leads to degradation of autoreactive CD8 T cells. *Proc. Natl. Acad. Sci.* **108**, 16735-16740 (2011).
46. P. Weigel, J. Oka, Temperature dependence of endocytosis mediated by the asialoglycoprotein receptor in isolated rat hepatocytes. Evidence for two potentially rate-limiting steps. *J. Biol. Chem.* **256**, 2615-2617 (1981).
47. Z. Eshhar, M. Ofarim, T. Waks, Generation of hybridomas secreting murine reagenic antibodies of α -DNP antibody specificity. *J. Immunol. Res.* **124**, 775-780 (1980).
48. K. Heller, P. Ochtrop, M. F. Albers, F. B. Zauner, A. Itzen, C. Hedberg, Covalent protein labeling by enzymatic phosphocholination. *Angew. Chem. Int. Ed. Engl.* **54**, 10327-10330 (2015).
49. J. Iglesias-Fernández, S. M. Hancock, S. S. Lee, M. Khan, J. Kirkpatrick, N. J. Oldham, K. McAuley, A. Fordham-Skelton, C. Rovira, B. G. Davis, A front-face ' S_N1 synthase' engineered from a retaining 'double- S_N2 ' hydrolase. *Nat. Chem. Bio.* **13**, 874 (2017).
50. P. C. Rensen, S. H. van Leeuwen, L. A. Sliedregt, T. J. van Berkel, E. A. Biessen, Design and synthesis of novel N-acetylgalactosamine-terminated glycolipids for targeting of lipoproteins to the hepatic asialoglycoprotein receptor. *J. Med. Chem.* **47**, 5798-5808 (2004).
51. N. Avlonitis, M. DeBunne, T. Aslam, N. McDonald, C. Haslett, K. Dhaliwal, M. Bradley, Highly specific, multi-branched fluorescent reporters for analysis of human neutrophil elastase. *Org. Biomol. Chem.* **11**, 4414-4418 (2013).
52. G. J. Miller, J. M. Gardiner, Adaptable synthesis of C-glycosidic multivalent carbohydrates and succinamide-linked derivatization. *Org. Lett.* **12**, 5262-5265 (2010).
53. J. A. Cisneros, M. J. Robertson, M. Valhondo, W. L. Jorgensen, A fluorescence polarization assay for binding to macrophage migration inhibitory factor and crystal structures for complexes of two potent inhibitors. *J. Am. Chem. Soc.* **138**, 8630-8638 (2016).
54. C. A. DeForest, D. A. Tirrell, A photoreversible protein-patterning approach for guiding stem cell fate in three-dimensional gels. *Nat. Mater.* **14**, 523-531 (2015).
55. L. Liao, J. Liu, E. C. Dreaden, S. W. Morton, K. E. Shopsowitz, P. T. Hammond, J. A. Johnson, A convergent synthetic platform for single-nanoparticle combination cancer therapy: ratiometric loading and controlled release of cisplatin, doxorubicin, and camptothecin. *J. Am. Chem. Soc.* **136**, 5896-5899 (2014).
56. D. M. Tian, J. Qiao, Y. Z. Bao, J. Liu, X. K. Zhang, X. L. Sun, Y. W. Zhang, X. S. Yao, J. S. Tang, Design and synthesis of biotinylated cardiac glycosides for probing Nur77 protein inducing pathway. *Bioorg. Med. Chem. Lett.* **29**, 707-712 (2019).

20200728 Supp .pdf (1.45 MiB)

[view on ChemRxiv](#) • [download file](#)

Title: Bifunctional small molecules that mediate the degradation of extracellular proteins

Authors: David F. Caianiello¹, Mengwen Zhang^{1,2}, Jason D. Ray¹, Jake C. Swartzel^{1,3}, Emily M. J. Branham¹, Egor Chirkin¹, Venkata R. Sabbasani¹, Angela Z. Gong¹, David M. McDonald¹, Viswanathan Muthusamy⁴, David A. Spiegel^{1,*}

Affiliations:

¹Department of Chemistry, Yale University. 225 Prospect Street, New Haven, CT 06511 (USA).

²Department of Molecular Biophysics and Biochemistry, Yale University. 266 Whitney Avenue, New Haven, CT 06511 (USA).

³Department of Molecular, Cellular, and Developmental Biology, Yale University. 260 Whitney Ave, New Haven, CT 06511 (USA).

⁴Yale Center for Precision Cancer Modeling, Yale University School of Medicine, New Haven, CT (USA).

*Correspondence to: david.spiegel@yale.edu

Abstract: Targeted protein degradation (TPD) has emerged as a promising and exciting therapeutic strategy. The majority of existing TPD technologies rely on the ubiquitin-proteasome system, and are therefore limited to targeting intracellular proteins. To address this limitation, we developed a class of modularly designed, bifunctional synthetic molecules called **MoDE-As** (**M**olecular **D**egraders of **E**xtracellular proteins through the **A**sialoglycoprotein receptor (ASGPR)), which are capable of mediating the degradation of extracellular proteins. MoDE-A molecules mediate the formation of a ternary complex between a target protein and the ASGPR, which is expressed primarily on hepatocytes. The target protein is then endocytosed and degraded by lysosomal proteases. We demonstrated the modularity of the MoDE-A technology by synthesizing bifunctional molecules that induce the degradation of both antibody and pro-inflammatory cytokine proteins. To our knowledge, these data represent the first experimental evidence that non-proteinogenic, synthetic molecules can be employed for the TPD of extracellular proteins both *in vitro* and *in vivo*. We believe that TPD mediated by the MoDE-A technology will have widespread applications for disease treatment.

One Sentence Summary: Bifunctional molecules that engage both a target protein and an endocytic receptor are able to induce the lysosomal degradation of extracellular proteins.

Main Text:

Extracellular protein levels are elevated in many different conditions, and technologies that mediate their removal from circulation have the potential to ameliorate a wide range of disease states (1, 2). One mechanism to decrease the serum concentration of an extracellular protein is to induce its endocytosis and subsequent degradation by lysosomal proteases. In order to accomplish

this goal, we developed a class of bifunctional molecules collectively termed **Molecular Degraders of Extracellular proteins** through the Asialoglycoprotein receptor (**MoDE-As**). MoDE-A molecules mediate the formation of a ternary complex between a target protein and the endocytic asialoglycoprotein receptor (ASGPR). The target protein is then endocytosed, trafficked to lysosomes, and degraded by lysosomal proteases (Figure 1A). To validate our technology, we focused on inducing the degradation of a model antibody that binds dinitrophenol (DNP). We also expanded our technology to induce the uptake of the cytokine macrophage migratory inhibitory factor (MIF), which is implicated in numerous inflammatory diseases (3). The bifunctional molecules developed through this work represent the first reported extracellular protein degrading technology validated *in vivo*.

We chose to degrade proteins via ASGPR-dependent mechanisms for several reasons. ASGPR is primarily expressed on hepatocytes, which are capable of catabolizing large quantities of protein with minimal toxicity compared to other cell types (4-8). Indeed, ASGPR controls the half-lives of several endogenous circulating proteins, including hormones (9), alkaline phosphatases (10), and proteins terminating in Sia α 2,6Gal glycans (11). ASGPR also plays a role in controlling the concentration of platelets in serum (12). Because of its well-defined binding requirements (13) and its abundant expression on hepatocytes, ASGPR has been used extensively to deliver therapeutic agents to the liver (14-18). Ligands for ASGPR are also readily available. Molecules that display multiple galactose-type sugars – such as the desialylated serum glycoproteins that aided in the discovery of ASGPR (19) – bind strongly to the receptor (20). For example, the ASGPR-binding trivalent GalNAc motif utilized in MoDE-A molecules, which is similar to those used in previous studies (21), is estimated to bind to multimeric ASGPR with K_d values in the low nanomolar range (22).

ASGPR mediates protein endocytosis through a well-studied mechanism. Each functional receptor is composed of two or more ASGPR protein chains, each with an extracellular C-type lectin domain with modest affinity to N-acetylgalactosamine (GalNAc) and related carbohydrates (23). Following endocytosis, ASGPR's binding to its sugar ligands is disrupted, and the dissociated protein ligand is trafficked to lysosomes where it is ultimately degraded by lysosomal proteases (24, 25).

The bifunctional MoDE-A molecules developed in this work contain three domains: an ASGPR-binding motif, a PEG spacer, and a protein-binding ligand (Figure 1A). D-MoDE-A and M-MoDE-A share the same ASGPR binding motif, but feature different target-binding termini (Figure 1B). To bind to α -DNP antibodies, D-MoDE-A contains a dinitrophenyl group connected through a PEG linker to the ASGPR-binding motif. In contrast, the MIF-binding molecule M-MoDE-A was synthesized by incorporating a carboxylic acid-terminated MIF tautomerase inhibitor with a K_d of approximately 53 nM (26). Full synthetic methods and characterization are available in the supporting information.

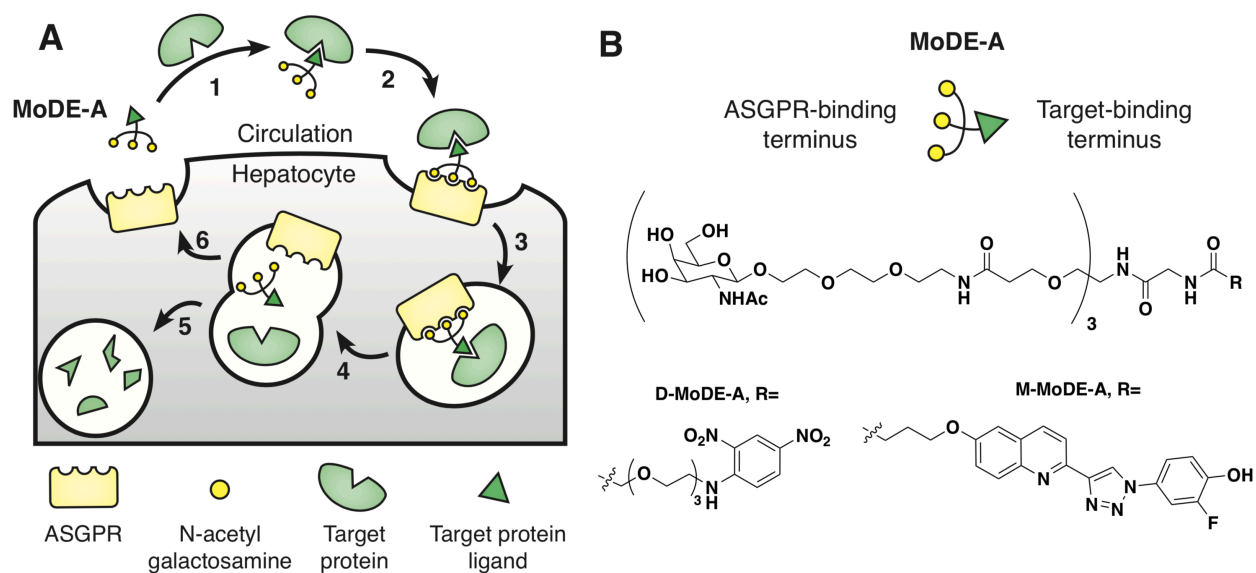


Figure 1: Bifunctional MoDE-A molecule design and chemical structures.

A) Schematic of uptake of target proteins via ASGPR mediated by MoDE-A bifunctional molecules.

B) Chemical structure of bifunctional molecules D-MoDE-A and M-MoDE-A.

We first sought to investigate whether D-MoDE-A could mediate the formation of a ternary complex between a fluorescently labeled α -DNP antibody and ASGPR on the surface of immortalized human hepatocyte HepG2 cells in suspension. The extent of fluorescently-labeled antibody association with cells was found to be dependent on the concentration of D-MoDE-A, with concentrations of 7.4 nM and 0.12 μ M eliciting half-maximal fluorescence association (Supplemental Figure 2A). The observed bell-shaped response to D-MoDE-A concentration is consistent with the prozone effect commonly observed in systems wherein a ternary complex is formed (27).

Cell-associated fluorescence was found to be inhibited by reagents that bind competitively to either ASGPR or α -DNP antibody (Supplemental Figure 2B). For example, we synthesized an antibody-binding negative control, DNP-OH3, which contains hydroxyl groups in place of GalNAc residues and is therefore not expected to engage ASGPR (Supplemental Figure 1A). Cellular fluorescence was decreased by increasing concentrations of both DNP-OH3 (IC_{50} = 36 nM) and monomeric GalNAc sugar (IC_{50} = 0.20 mM) (Supplemental Figure 2B). Proteins that bind specifically to ASGPR also decreased D-MoDE-A-mediated cellular fluorescence (Figure 2A). Fetuin (28) and orosomucoid (ORM) (29) are serum glycoproteins that bind to ASGPR only after they have been desialylated to produce asialofetuin (ASF, K_i = 17 nM) and asialoorosomucoid (ASOR, K_i = 1.7 nM), respectively (30). Both ASF (IC_{50} = 65 nM) and ASOR (IC_{50} = 17 nM) decreased cellular fluorescence, while fetuin and ORM did not. Taken together, these data suggest that D-MoDE-A mediates the formation of a ternary complex between α -DNP antibody and ASGPR on the hepatocyte surface.

We next explored whether D-MoDE-A mediates the endocytosis of fluorescently labeled α -DNP antibody. We observed that the intracellular fluorescence of adherent HepG2 cells was dependent on the concentration of both D-MoDE-A and antibody (Figure 2B), and that fluorescence increased over time (Supplemental Figure 2C). This observed increase in intracellular fluorescence was inhibitable by reagents that were previously shown to interfere with ternary complex formation (Figure 2C). As expected, we did not observe a significant decrease in antibody uptake when cells were treated with the proteins ORM or fetuin, which do not bind strongly to ASGPR. These data are consistent with a model in which D-MoDE-A mediates antibody uptake by engaging ASGPR.

In order to determine whether bifunctional small molecule-mediated endocytosis via ASGPR is generalizable to other proteins of interest, we conducted similar experiments with M-MoDE-A and fluorescently labeled human MIF protein (Figure 2D). We observed increased intracellular fluorescence with increasing concentrations of M-MoDE-A, with maximal fluorescence observed at the highest concentration we investigated (1.0 μ M). In contrast to D-MoDE-A, we did not observe a prozone effect with M-MoDE-A-mediated MIF uptake. These data support that the MoDE-A approach can be generalized to proteins other than α -DNP antibody.

To explore the cellular mechanism of antibody uptake, we next treated cells with chemical inhibitors of several endocytic pathways (Figure 2E). Combined treatment with the global endocytosis inhibitors sodium azide and 2-deoxyglucose (DOG) (31) significantly decreased intracellular fluorescence. Fluorescence was also significantly decreased by reagents that inhibit clathrin-dependent endocytosis by disrupting endosomal formation (sucrose (32)) and/or acidification (bafilomycin (33), chloroquine (33), and monensin (34)). In contrast, inhibitors of

caveolae-mediated endocytosis (nystatin (35)) and macropinocytosis and phagocytosis (cytochalasin D (36), 5-(N-Ethyl-N-isopropyl)amiloride (EIPA), and amiloride (37)) did not significantly decrease cellular fluorescence. The pattern of inhibition observed in these experiments is consistent with an endocytic mechanism that relies on clathrin, but not other endocytic pathways. Given that previous reports have shown that endocytosis mediated by ASGPR is dependent on clathrin (38, 39), this data further supports ASGPR's participation in antibody endocytosis mediated by D-MoDE-A.

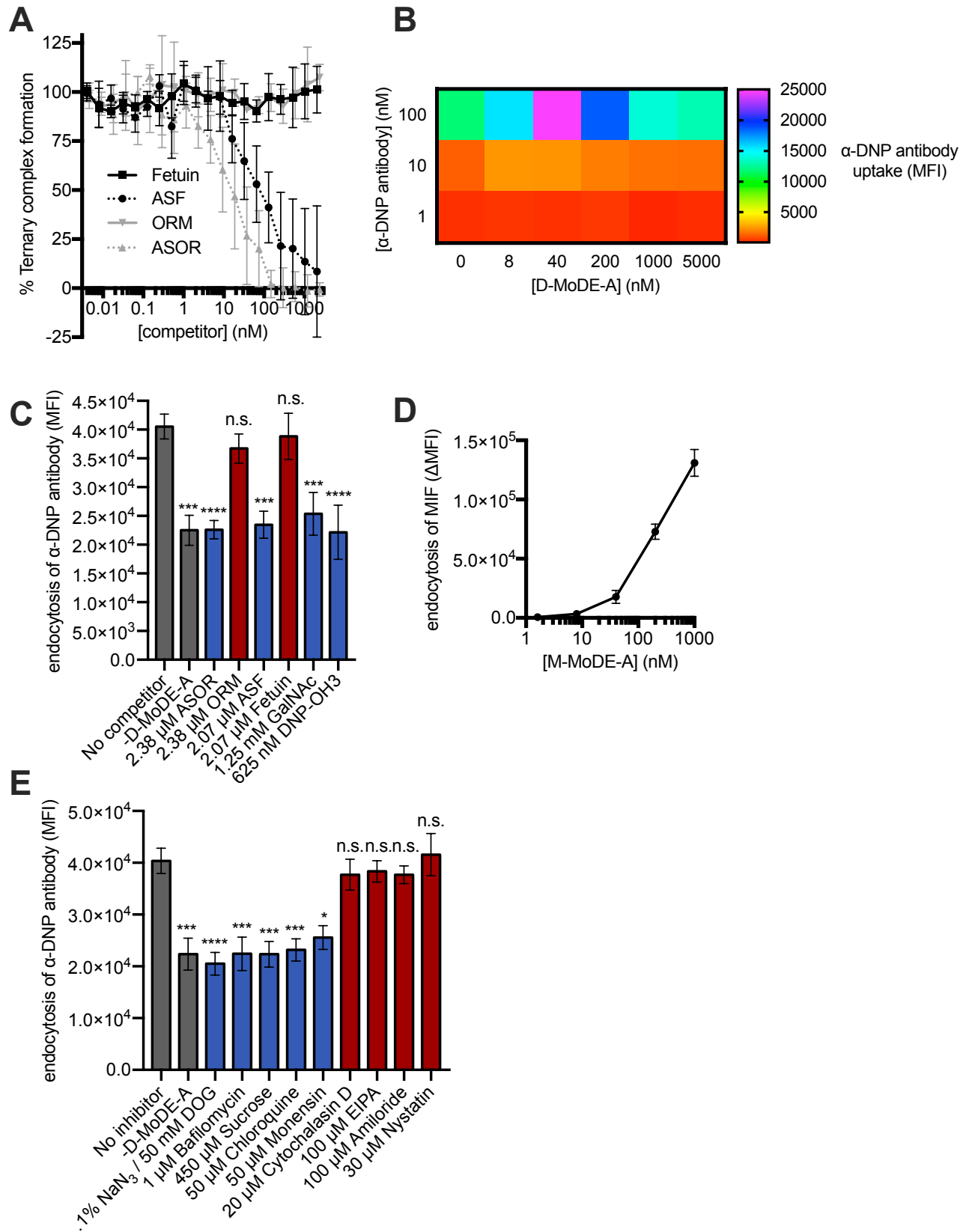


Figure 2: Bifunctional MoDE-A molecules mediate endocytosis of target proteins

A) Ternary complex formation mediated by D-MoDE-A is inhibited by known ASGPR-binding proteins asialofetuin and asialoorosomucoid.

B) Intracellular fluorescence is dependent on the concentrations of both α -DNP antibody and D-MoDE-A (6 hour incubation).

C) Endocytosis mediated by D-MoDE-A is decreased by competitive binders of either ASGPR or α -DNP antibody. Controls are grey, compounds expected to inhibit the proposed mode of action of D-MoDE-A are blue, and compounds not expected to inhibit are red. Data are presented as mean \pm SD of 9 replicates over four experiments. Statistical differences were determined by Kruskal-Wallis test with post-hoc comparisons between each inhibitor and the no-inhibitor group (* $P < 0.05$, ** $P < 0.01$, *** $P < 0.0001$, **** $P < 0.0001$, “n.s.” $P > 0.9999$).

D) Endocytosis of fluorescently labeled MIF is dependent on M-MoDE-A concentration.

E) Inhibitors of clathrin-dependent endocytosis decrease D-MoDE-A-mediated α -DNP antibody uptake. Data are presented as mean \pm SD of 9 replicates over four experiments. Statistics were performed as outlined in Figure 2C.

Having demonstrated that D-MoDE-A mediates the endocytosis of α -DNP antibodies, we sought to investigate the subcellular localization of endocytosed fluorescently labeled α -DNP antibody. Intracellular antibody-derived fluorescence was found to depend on the presence of both D-MoDE-A and α -DNP antibody (Supplemental Figure 3A). We did not observe colocalization of endocytosed antibody with the early endosome marker EEA1 in cells (Figure 3A). In contrast, we observed strong colocalization of antibody with the lysosome membrane protein LAMP2 (Figure 3B). Taken together, these microscopy data suggest that trafficking to lysosomes is rapid on the time scale of this experiment (40) and that the majority of endocytosed antibody was present in mature endocytic compartments.

In addition, we used western blotting with an antibody directed to Alexa Fluor 488 to determine if endocytosed fluorescently labeled α -DNP antibodies are degraded *in vitro*. Lysates from HepG2 cells treated with both D-MoDE-A and α -DNP antibody were found to accumulate fluorophore in a time- and D-MoDE-A-dependent manner (Figure 3C). Alexa Fluor 488 in cell lysates was associated with only full-length antibody after two hours of incubation. After six hours, a lower molecular weight fluorophore-associated protein fragment between 37 and 50 kDa began to appear. An additional protein fragment with a molecular weight between 25 and 37 kDa was also observed after 24 hours. We believe that these fluorophore-associated protein fragments are degradation products resulting from lysosomal proteolysis of α -DNP antibodies, collectively indicating that endocytosed antibody is degraded in HepG2 cells. Furthermore, no degradation products were observed in the cell supernatant (Supplemental Figure 3B) suggesting that antibody degradation is taking place in or on HepG2 cells. Together with the above immunofluorescence studies showing colocalization of antibody-derived fluorescence with lysosomes, these studies support that antibody degradation is mediated by lysosomal proteases. Lysosomal degradation is further consistent with a mechanism dependent on ASGPR.

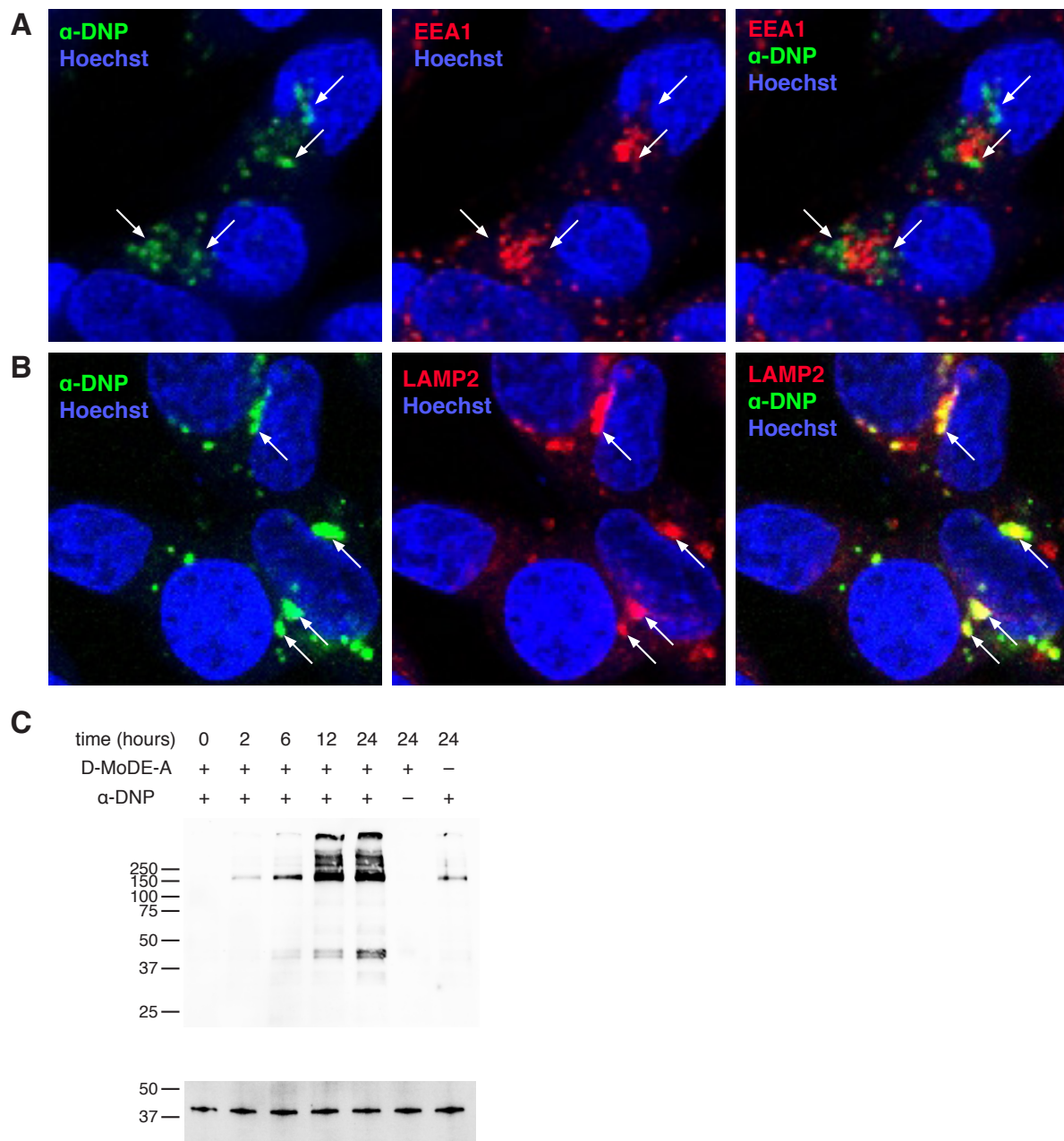


Figure 3: Target protein α -DNP antibody is trafficked to lysosomes and degraded

A) Endocytosed α -DNP antibody does not colocalize with the early endosome marker EEA1.

5 B) Endocytosed α -DNP antibody colocalizes with the late endosome and lysosome protein LAMP2.

C) Representative western blot showing accumulation of antibody-derived protein fragments in cell lysates.

Having demonstrated that D-MoDE-A mediates the degradation of α -DNP antibodies *in vitro*, we sought to evaluate the viability of the MoDE-A technology *in vivo*. A dose of 1 mpk D-MoDE-A was found to be bioavailable via IP dosing in nude mice, with the maximal serum concentration reached after 1 h and a measured half-life in serum of 0.67 h. D-MoDE-A was well-tolerated up to doses of 100 mpk, with no significant differences in body weight or serum liver enzyme levels between control and treatment groups (Supplemental Figure 4A-C). These results supported the suitability of D-MoDE-A for more detailed studies *in vivo*.

Treatment with D-MoDE-A was found to accelerate the depletion of monoclonal mouse IgG2 α -DNP antibodies from serum in nude mice *in vivo* (Figure 4A). Following an initial dose of 200 μ g α -DNP antibody, both daily and twice-daily injections of 1 mpk D-MoDE-A significantly reduced antibody levels compared to PBS treatment over 21 days. Daily treatment with D-MoDE-A also gave a significant decrease in antibody levels following an initial antibody dose of 500 μ g, indicating that D-MoDE-A is effective over a range of target protein concentrations *in vivo*.

We did not observe accelerated antibody depletion from serum following treatment with the negative control compound DNP-OH3, which binds to α -DNP antibody but not ASGPR. Treatment with 10 mpk of DNP-OH3 did not lead to accelerated antibody depletion from serum (Figure 4B), supporting that ASGPR binding is required for target protein depletion *in vivo*. Unexpectedly, a dose of 100 mpk DNP-OH3 resulted in a small but statistically significant decrease in antibody clearance compared to the PBS control. We hypothesize that this is a result of an increase in the antibody's hydrodynamic radius due to the DNP-OH3 PEG chains, which may increase its half-life *in vivo*. Related phenomena have been widely observed for pegylated proteins, and have been exploited for increasing the half lives of various therapeutic modalities (41).

Single doses of D-MoDE-A were also found to be efficacious at mediating α -DNP antibody depletion, albeit less effectively than daily dosing (Supplemental Figure 4D). Treatment with either 1 mpk or 10 mpk D-MoDE-A were found to be the most effective, with 52% and 34% of α -DNP antibody depleted from serum respectively 24 hours after a single dose, versus 24% depletion in the vehicle control. Significant depletion was also observed following a dose of 100 mpk of D-MoDE-A. We therefore concluded that D-MoDE-A is able to mediate the depletion of a monoclonal antibody from serum, and functions across a wide range of target protein concentrations and dosing regimens.

D-MoDE-A was also found to be efficacious in depleting polyclonal α -DNP antibody from serum collected from mice immunized with DNP-KLH (Figure 4C). Following daily treatment with D-MoDE-A, significantly more polyclonal α -DNP antibody was removed from serum compared to the PBS control at each time point. Thus, the small molecule D-MoDE-A is not restricted in function to only monoclonal mouse antibodies, but is also effective at removing polyclonal α -DNP antibodies from circulation in mice.

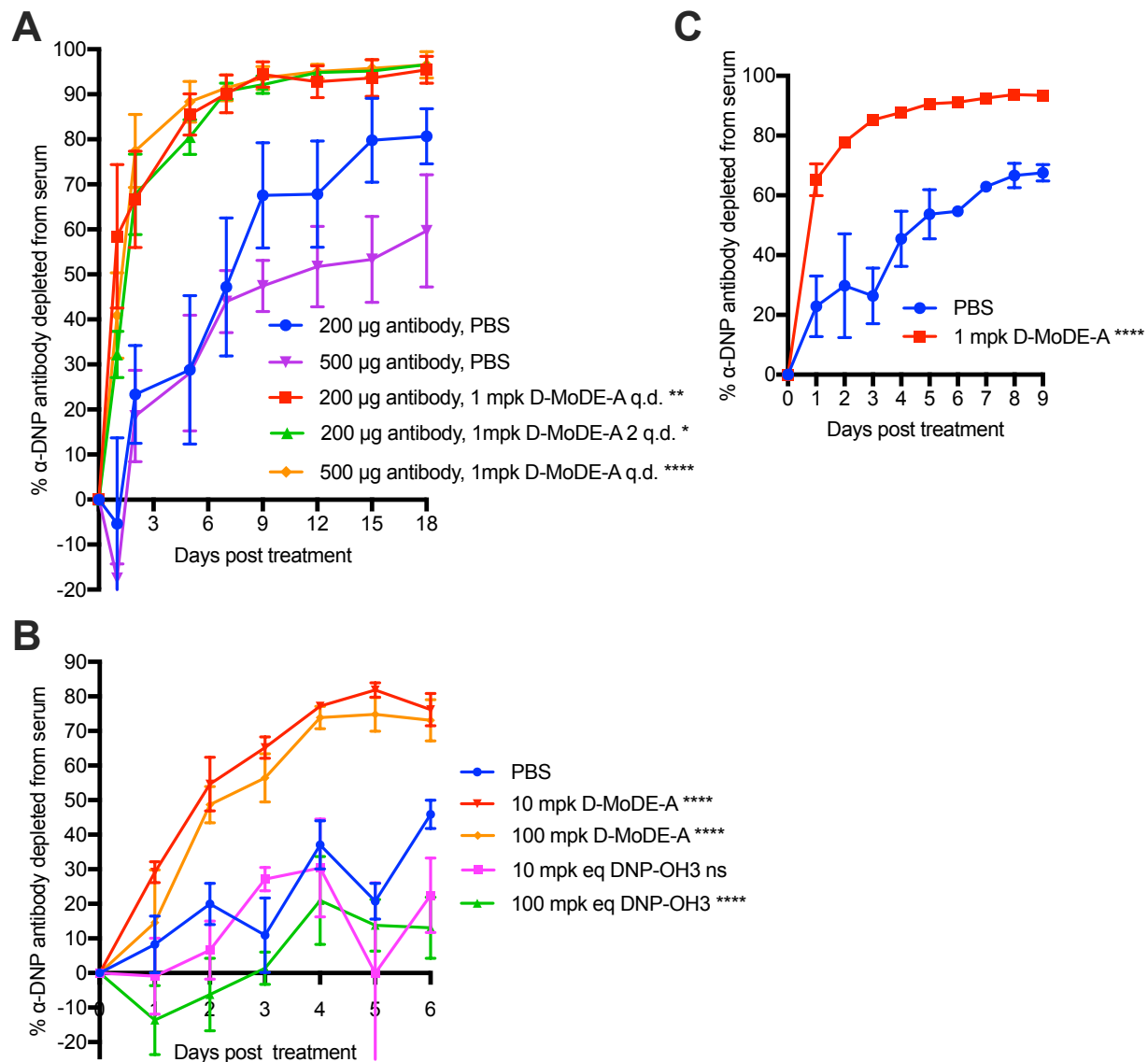


Figure 4: D-MoDE-A mediates the accelerated depletion of α -DNP antibodies from serum *in vivo*

- 5 A) Serum levels of α -DNP antibody as measured by ELISA decrease more rapidly following repeated treatment with D-MoDE-A. Each experimental group contained three mice. Statistical differences in experiments involving *in vivo* depletion of α -DNP antibody were assessed by repeated measures two-way ANOVA with Tukey's tests for post-hoc comparison of simple effects between each of the treatment groups and PBS.
- 10 B) Significant decreases in serum levels of α -DNP antibody are observed after treatment with D-MoDE-A, but not DNP-OH3. Each experimental group contained at least five mice.
- C) Treatment with D-MoDE-A decreases serum levels of polyclonal α -DNP antibody. The PBS treated group contained two mice, while the D-MoDE-A group contained three mice.

To our knowledge, the MoDE-A technology represents the first demonstration that non-proteinogenic synthetic molecules can effectively mediate the degradation of extracellular proteins. The data presented herein demonstrate that such molecules can induce targeted degradation of structurally diverse proteins, both in tissue culture and *in vivo*. Recently, Bertozzi and colleagues disclosed the lysosome targeting chimeras (LYTACs) technology, an elegant approach for degrading extracellular and cell surface proteins (42). LYTACs comprise antibodies modified with polymeric ligands of the cation independent mannose-6-phosphate receptor (CI-M6PR). Although we believe that the LYTAC approach will likely complement what we present herein, MoDE-A compounds possess several advantages: they are relatively small in size, monodisperse, and non-protein based. These attributes are expected to facilitate synthesis and rapid application to targeting other proteins of interest.

The therapeutic potential of small molecule-based approaches to TPD are particularly evident in light of the recent clinical development of proteolysis targeting chimeras (PROTACs) (43). PROTACs and related technologies induce the formation of ternary complexes between target proteins and E3 ligases such that target proteins are ubiquitinated and subsequently degraded by the proteasome. Due to their mechanism, however, PROTACs have a critical limitation: they cannot degrade targets that are not exposed to the cytosol.

The MoDE-A compounds developed in this work expand the possible targets of small-molecule mediated protein degradation substantially by expanding the scope of TPD to non-cytosolic, extracellular proteins. We believe that MoDE-A compounds will be particularly effective because they direct proteins targets primarily to hepatocytes, a cell type equipped to catabolize large amounts of endocytosed proteins. Furthermore, evidence suggests that ASGPR is tolerogenic immunologically (44, 45), which would minimize the likelihood of inducing autoimmune responses to targeted proteins. We expect that the positive pharmacological and biological characteristics of MoDE-A compounds, as well as the straightforward, modular synthetic routes we have developed for their syntheses, will enable rapid optimization and adoption of the MoDE-A technology in diverse, disease-relevant contexts.

Data and materials availability: All data is available in the main text or the supplementary materials.

Supplementary Materials:

- 5 Biological Materials and Methods
- Synthetic Methods
- Figures S1-S4
- Spectral Data
- Full reference list

10

Acknowledgments: We thank C. Paulsen and S. Miller for use of equipment; the Eshhar Lab for providing hybridomas for antibody production; and A. Phillips for helpful comments during the preparation of this manuscript.

- 15 **Funding:** We are thankful for financial support from the National Institute of Health Yale Chemical Biology Training Grant to JDR (2T32GM06754 3-17), EMJB (5T32GM06754 3-12), and DFC (T32GM067543), the Department of Defense (BC120554), and Yale University (Michele Dufault Summer Research Fellowship to AZG).

- 20 **Competing Interests:** This work is the subject of two published patents: PCT/US2019/26239 and PCT/US2019/26260. DAS is a founder of and has equity in Kleo Pharmaceuticals, an entity focused on the development of bifunctional molecules. DAS also receives honoraria for consulting for Kleo. Kleo has licensed intellectual property from DAS, which is used in this research.

References and Notes:

1. B. Chen, X. Shi, Y. Cui, A. Hou, P. Zhao, A Review of PCSK9 Inhibitors and their Effects on Cardiovascular Diseases. *Curr. Top. Med. Chem.* **19**, 1790-1817 (2019).
2. G. D. Kalliolias, L. B. Ivashkiv, TNF biology, pathogenic mechanisms and emerging therapeutic strategies. *Nat. Rev. Rheumatol.* **12**, 49 (2016).
3. J. B. Bilsborrow, E. Doherty, P. V. Tilstam, R. Bucala, Macrophage migration inhibitory factor (MIF) as a therapeutic target for rheumatoid arthritis and systemic lupus erythematosus. *Expert Opin. Ther.* **23**, 733-744 (2019).
4. J. Martínez-Fábregas, A. Prescott, S. van Kasteren, D. L. Pedrioli, I. McLean, A. Moles, T. Reinheckel, V. Poli, C. Watts, Lysosomal protease deficiency or substrate overload induces an oxidative-stress mediated STAT3-dependent pathway of lysosomal homeostasis. *Nat. Commun.* **9**, 5343 (2018).
5. C. Zoja, A. Benigni, G. Remuzzi, Protein overload activates proximal tubular cells to release vasoactive and inflammatory mediators. *Nephron Exp. Nephrol.* **7**, 420-428 (1999).
6. H. Nakajima, M. Takenaka, J. Y. Kaimori, T. Hamano, H. Iwatani, T. Sugaya, T. Ito, M. Hori, E. Imai, Activation of the signal transducer and activator of transcription signaling pathway in renal proximal tubular cells by albumin. *J. Am. Soc. Nephrol.* **15**, 276-285 (2004).
7. M. Tanowitz, L. Hettrick, A. Revenko, G. A. Kinberger, T. P. Prakash, P. P. Seth, Asialoglycoprotein receptor 1 mediates productive uptake of N-acetylgalactosamine-conjugated and unconjugated phosphorothioate antisense oligonucleotides into liver hepatocytes. *Nucleic Acids Res.* **45**, 12388-12400 (2017).
8. P. K. Grewal, "The Ashwell-Morell Receptor" in *Methods in Enzymology*. (Elsevier, 2010), vol. 479, pp. 223-241.
9. Y. Mi, A. Lin, D. Fiete, L. Steirer, J. U. Baenziger, Modulation of mannose and asialoglycoprotein receptor expression determines glycoprotein hormone half-life at critical points in the reproductive cycle. *J. Biol. Chem.* **289**, 12157-12167 (2014).
10. W. H. Yang, P. V. Aziz, D. M. Heithoff, M. J. Mahan, J. W. Smith, J. D. Marth, An intrinsic mechanism of secreted protein aging and turnover. *Proc. Natl. Acad. Sci.* **112**, 13657-13662 (2015).
11. L. M. Steirer, E. I. Park, R. R. Townsend, J. U. Baenziger, The asialoglycoprotein receptor regulates levels of plasma glycoproteins terminating with sialic acid α 2, 6-galactose. *J. Biol. Chem.* **284**, 3777-3783 (2009).
12. R. Grozovsky, A. J. Begonja, K. Liu, G. Visner, J. H. Hartwig, H. Falet, K. M. Hoffmeister, The Ashwell-Morell receptor regulates hepatic thrombopoietin production via JAK2-STAT3 signaling. *Nat. Med.* **21**, 47 (2015).
13. X. Huang, J. C. Leroux, B. Castagner, Well-defined multivalent ligands for hepatocytes targeting via asialoglycoprotein receptor. *Bioconjugate Chem.* **28**, 283-295 (2016).
14. A. A. D'Souza, P. V. Devarajan, Asialoglycoprotein receptor mediated hepatocyte targeting—strategies and applications. *J. Control. Release* **203**, 126-139 (2015).
15. S. Matsuda, K. Keiser, J. K. Nair, K. Charisse, R. M. Manoharan, P. Kretschmer, C. G. Peng, A. V. Kel'in, P. Kandasamy, J. L. S. Willoughby, A. Liebow, W. Querbes, K. Yucius, T. Nguyen, S. Milstein, M. A. Maier, K. G. Rajeev, M. Manoharan, siRNA conjugates carrying sequentially assembled trivalent N-acetylgalactosamine linked

through nucleosides elicit robust gene silencing in vivo in hepatocytes. *ACS Chem. Biol.* **10**, 1181-1187 (2015).

16. E. A. Biessen, A. R. Valentijn, R. L. De Vruhe, E. Van De Bilt, L. A. Sliedregt, P. Prince, M. K. Bijsterbosch, J. H. Van Boom, G. A. Van Der Marel, P. J. Abrahams, T. J. Van Berkel, Novel hepatotrophic prodrugs of the antiviral nucleoside 9-(2-phosphonylmethoxyethyl) adenine with improved pharmacokinetics and antiviral activity. *FASEB J.* **14**, 1784-1792 (2000).
17. A. M. Pujol, M. Cuillel, O. Renaudet, C. Lebrun, P. Charbonnier, D. Cassio, C. Gateau, P. Dumy, E. Mintz, P. Delangle, Hepatocyte targeting and intracellular copper chelation by a thiol-containing glycocyclopeptide. *J. Am. Chem. Soc.* **133**, 286-296 (2010).
18. A. Akinc, W. Querbes, S. De, J. Qin, M. Frank-Kamenetsky, K. N. Jayaprakash, M. Jayaraman, K. G. Rajeev, W. L. Cantley, J. R. Dorkin, J. S. Butler, L. Qin, T. Racie, A. Sprague, E. Fava, A. Zeigerer, M. J. Hope, M. Zerial, D. W. Y. Sah, K. Fitzgerald, M. A. Tracy, M. Manoharan, V. Kotliansky, A. de Fuogerolles, M. A. Maier, Targeted delivery of RNAi therapeutics with endogenous and exogenous ligand-based mechanisms. *Mol. Ther.* **18**, 1357-1364 (2010).
19. V. Bocci, The role of sialic acid in determining the life-span of circulating cells and glycoproteins. *Experientia* **32**, 135-140 (1976).
20. J. U. Baenziger, D. Fiete, Galactose and N-acetylgalactosamine-specific endocytosis of glycopeptides by isolated rat hepatocytes. *Cell* **22**, 611-620 (1980).
21. J. R. Merwin, G. S. Noell, W. L. Thomas, H. C. Chiou, M. E. DeRome, T. D. McKee, G. L. Spitalny, M. A. Findeis, Targeted delivery of DNA using YEE (GalNAcAH)₃, a synthetic glycopeptide ligand for the asialoglycoprotein receptor. *Bioconjugate Chem.* **5**, 612-620 (1994).
22. P.C. Rensen, L. A. Sliedregt, M. Ferns, E. Kieviet, S. M. Van Rossenberg, S. H. van Leeuwen, T. J. Van Berkel, E. A. Biessen, Determination of the upper size limit for uptake and processing of ligands by the asialoglycoprotein receptor on hepatocytes *in vitro* and *in vivo*. *J. Biol. Chem.* **276**, 37577-37584 (2001).
23. S. K. Mamidyalala, S. Dutta, B. A. Chrnyk, C. Prévaille, H. Wang, J. M. Withka, A. McColl, T. A. Subashi, S. J. Hawrylik, M. C. Griffor, S. Kim, J. A. Pfefferkorn, D. A. Price, E. Menhaji-Klotz, V. Mascitti, M. G. Finn, Glycomimetic ligands for the human asialoglycoprotein receptor. *J. Am. Chem. Soc.* **134**, 1978-1981 (2012).
24. T. Onizuka, H. Shimizu, Y. Moriwaki, T. Nakano, S. Kanai, I. Shimada, H. Takahashi, NMR study of ligand release from asialoglycoprotein receptor under solution conditions in early endosomes. *FEBS J.* **279**, 2645-2656 (2012).
25. J. H. LaBadie, K. P. Chapman, N. N. Aronson, Glycoprotein catabolism in rat liver: Lysosomal digestion of iodinated asialo-fetuin. *Biochem. J.* **152**, 271-279 (1975).
26. J. A. Cisneros, M. J. Robertson, M. Valhondo, W. L. Jorgensen, A fluorescence polarization assay for binding to macrophage migration inhibitory factor and crystal structures for complexes of two potent inhibitors. *J. Am. Chem. Soc.* **138**, 8630-8638 (2016).
27. E. F. Douglass Jr, C. J. Miller, G. Sparer, H. Shapiro, D. A. Spiegel, A comprehensive mathematical model for three-body binding equilibria. *J. Am. Chem. Soc.* **135**, 6092-6099 (2013).
28. W. Brown, N. Saunders, K. Møslgård, K. Dziegielewska, Fetuin—an old friend revisited. *BioEssays* **14**, 749-755 (1992).

29. C. L. Fernandes, R. Ligabue-Braun, H. Verli, Structural glycobiology of human α_1 -acid glycoprotein and its implications for pharmacokinetics and inflammation. *Glycobiology* **25**, 1125-1133 (2015).
30. B. Shi, M. Abrams, L. Sepp-Lorenzino, Expression of Asialoglycoprotein Receptor 1 in Human Hepatocellular Carcinoma. *J Histochem. Cytochem.* **61**, 901-909 (2013).
31. A. Cooper, Y. Shaul, Clathrin-mediated endocytosis and lysosomal cleavage of hepatitis B virus capsid-like core particles. *J. Biol. Chem.* **281**, 16563-16569 (2006).
32. S. Guo, X. Zhang, M. Zheng, X. Zhang, C. Min, Z. Wang, S. H. Cheon, M. H. Oak, S. Y. Nah, K. M. Kim, Selectivity of commonly used inhibitors of clathrin-mediated and caveolae-dependent endocytosis of G protein-coupled receptors. *BBA-Biomembranes* **1848**, 2101-2110 (2015).
33. L. D. Cervia, C. C. Chang, L. Wang, F. Yuan, Distinct effects of endosomal escape and inhibition of endosomal trafficking on gene delivery via electrotransfection. *PloS One* **12** (2017).
34. R. Ippoliti, P. Ginobbi, E. Lendaro, I. D'Agostino, D. Ombres, P. A. Benedetti, M. Brunori, G. Citro, The effect of monensin and chloroquine on the endocytosis and toxicity of chimeric toxins. *Cell. Mol. Life Sci.* **54**, 866-875 (1998).
35. Q. Ba, N. Zhou, J. Duan, T. Chen, M. Hao, X. Yang, J. Li, J. Yin, R. Chu, H. Wang, Dihydroartemisinin exerts its anticancer activity through depleting cellular iron via transferrin receptor-1. *PloS One* **7** (2012).
36. M. M. Zegers, K. J. Zaal, S. C. van IJzendoorn, K. Klappe, D. Hoekstra, Actin filaments and microtubules are involved in different membrane traffic pathways that transport sphingolipids to the apical surface of polarized HepG2 cells. *Mol. Biol. Cell* **9**, 1939-1949 (1998).
37. R. Maidorn, E. Cragoe, I. Tannock, Therapeutic potential of analogues of amiloride: inhibition of the regulation of intracellular pH as a possible mechanism of tumour selective therapy. *Br. J. Cancer* **67**, 297-303 (1993).
38. J. Oka, M. Christensen, P. Weigel, Hyperosmolarity inhibits galactosyl receptor-mediated but not fluid phase endocytosis in isolated rat hepatocytes. *J. Biol. Chem.* **264**, 12016-12024 (1989).
39. A. L. Schwartz, A. Bolognesi, S. E. Fridovich, Recycling of the asialoglycoprotein receptor and the effect of lysosomotropic amines in hepatoma cells. *J. Cell Biol.* **98**, 732-738 (1984).
40. K. Bridges, J. Harford, G. Ashwell, R. D. Klausner, Fate of receptor and ligand during endocytosis of asialoglycoproteins by isolated hepatocytes. *Proc. Natl. Acad. Sci.* **79**, 350-354 (1982).
41. S. Jevsevar, M. Kunstelj, "Half-life extension through PEGylation" in *Therapeutic Proteins: Strategies to Modulate Their Plasma Half-lives*, R. Kontermann, Ed. (Wiley-Blackwell, 2012), chap. 3.
42. S. Banik, K. Pedram, S. Wisnovsky, N. Riley, C. Bertozzi, https://chemrxiv.org/articles/preprint/Lysosome_Targeting_Chimeras_LYTACs_for_the_Degradation_of_Secreted_and_Membrane_Proteins/7927061/2 (2019).
43. X. Sun, H. Gao, Y. Yang, M. He, Y. Wu, Y. Song, Y. Tong, Y. Rao, PROTACs: great opportunities for academia and industry. *Sig. Transduct. Target Ther.* **4**, 64 (2019).
44. C. S. Guy, S. L. Rankin, T. I. Michalak, Hepatocyte cytotoxicity is facilitated by asialoglycoprotein receptor. *Hepatol.* **54**, 1043-1050 (2011).

45. V. Benseler, A. Warren, M. Vo, L. E. Holz, S. S. Tay, D. G. Le Couteur, E. Breen, A. C. Allison, N. van Rooijen, C. McGuffog, H. J. Schlitt, D. G. Bowen, G. W. McCaughan, P. Bertolino, Hepatocyte entry leads to degradation of autoreactive CD8 T cells. *Proc. Natl. Acad. Sci.* **108**, 16735-16740 (2011).
- 5 46. P. Weigel, J. Oka, Temperature dependence of endocytosis mediated by the asialoglycoprotein receptor in isolated rat hepatocytes. Evidence for two potentially rate-limiting steps. *J. Biol. Chem.* **256**, 2615-2617 (1981).
47. Z. Eshhar, M. Ofarim, T. Waks, Generation of hybridomas secreting murine reagenic antibodies of anti-DNP specificity. *J. Immunol. Res.* **124**, 775-780 (1980).
- 10 48. K. Heller, P. Ochtrop, M. F. Albers, F. B. Zauner, A. Itzen, C. Hedberg, Covalent protein labeling by enzymatic phosphocholination. *Angew. Chem. Int. Ed. Engl.* **54**, 10327-10330 (2015).
49. J. Iglesias-Fernández, S. M. Hancock, S. S. Lee, M. Khan, J. Kirkpatrick, N. J. Oldham, K. McAuley, A. Fordham-Skelton, C. Rovira, B. G. Davis, A front-face 'S_Ni synthase' engineered from a retaining 'double-S_N2' hydrolase. *Nat. Chem. Bio.* **13**, 874 (2017).
- 15 50. P. C. Rensen, S. H. van Leeuwen, L. A. Sliedregt, T. J. van Berkel, E. A. Biessen, Design and synthesis of novel N-acetylgalactosamine-terminated glycolipids for targeting of lipoproteins to the hepatic asialoglycoprotein receptor. *J. Med. Chem.* **47**, 5798-5808 (2004).
- 20 51. N. Avlonitis, M. DeBunne, T. Aslam, N. McDonald, C. Haslett, K. Dhaliwal, M. Bradley, Highly specific, multi-branched fluorescent reporters for analysis of human neutrophil elastase. *Org. Biomol. Chem.* **11**, 4414-4418 (2013).
52. G. J. Miller, J. M. Gardiner, Adaptable synthesis of C-glycosidic multivalent carbohydrates and succinamide-linked derivatization. *Org. Lett.* **12**, 5262-5265 (2010).
- 25 53. J. A. Cisneros, M. J. Robertson, M. Valhondo, W. L. Jorgensen, A fluorescence polarization assay for binding to macrophage migration inhibitory factor and crystal structures for complexes of two potent inhibitors. *J. Am. Chem. Soc.* **138**, 8630-8638 (2016).
54. C. A. DeForest, D. A. Tirrell, A photoreversible protein-patterning approach for guiding stem cell fate in three-dimensional gels. *Nat. Mater.* **14**, 523-531 (2015).
- 30 55. L. Liao, J. Liu, E. C. Dreaden, S. W. Morton, K. E. Shopsowitz, P. T. Hammond, J. A. Johnson, A convergent synthetic platform for single-nanoparticle combination cancer therapy: ratiometric loading and controlled release of cisplatin, doxorubicin, and camptothecin. *J. Am. Chem. Soc.* **136**, 5896-5899 (2014).
- 35 56. D. M. Tian, J. Qiao, Y. Z. Bao, J. Liu, X. K. Zhang, X. L. Sun, Y. W. Zhang, X. S. Yao, J. S. Tang, Design and synthesis of biotinylated cardiac glycosides for probing Nur77 protein inducing pathway. *Bioorg. Med. Chem. Lett.* **29**, 707-712 (2019).

20200731 main.pdf (1.28 MiB)

[view on ChemRxiv](#) • [download file](#)
